Neural Networks 184 (2025) 107020

Contents lists available at ScienceDirect

Neural Networks

journal homepage: www.elsevier.com/locate/neunet

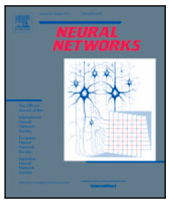

Full Length Article

# Fusion of brain imaging genetic data for alzheimer's disease diagnosis and causal factors identification using multi-stream attention mechanisms and graph convolutional networks

Wei Peng [a,b,*], Yanhan Ma [a,b,1], Chunshan Li [a,b,1], Wei Dai [a,b], Xiaodong Fu [a,b], Li Liu [a,b], Lijun Liu [a,b], Jin Liu [c]

[a] Faculty of Information Engineering and Automation, Kunming University of Science and Technology; Kunming 650500, PR China
[b] Computer Technology Application Key Lab of Yunnan Province; Kunming 650500, PR China
[c] Hunan Provincial Key Lab on Bioinformatics, School of Computer Science and Engineering, Central South University, Changsha 410083, PR China

ARTICLE INFO

Dataset link: https://adni.loni.usc.edu/, https://github.com/weiba/MCAGCN

*Keywords:*
Multimodal fusion
Alzheimer's disease diagnosis
Brain imaging genetics
Multi-stream attention
Graph convolutional network

ABSTRACT

Correctly diagnosing Alzheimer's disease (AD) and identifying pathogenic brain regions and genes play a vital role in understanding the AD and developing effective prevention and treatment strategies. Recent works combine imaging and genetic data, and leverage the strengths of both modalities to achieve better classification results. In this work, we propose MCA-GCN, a Multi-stream Cross-Attention and Graph Convolutional Network-based classification method for AD patients. It first constructs a brain region-gene association network based on brain region fMRI time series and gene SNP data. Then it integrates the absolute and relative positions of the brain region time series to obtain a new brain region time series containing temporal information. Then long-range and local association features between brain regions and genes are sequentially aggregated by multi-stream cross-attention and graph convolutional networks. Finally, the learned brain region and gene features are input to the fully connected network to predict AD types. Experimental results on the ADNI dataset show that our model outperforms other methods in AD classification tasks. Moreover, MCA-GCN designed a multi-stage feature scoring process to extract high-risk genes and brain regions related to disease classification.

## 1. Introduction

Alzheimer's disease (AD) is a chronic neurodegenerative disease that is a form of dementia. It causes severe impairments in memory, thinking skills, mobility, and language (Bellenguez et al., 2022). In addition to the huge impact of this disease on the patients themselves, it also burdens their families and society. Since no effective cure has been found, it is important to correctly diagnose Alzheimer's disease and identify the corresponding brain regions and genes to prevent and treat AD (Yu, Sporns, & Saykin, 2021).

Brain imaging genetics is an emerging field that combines brain imaging techniques, such as structural magnetic resonance imaging (sMRI) and functional magnetic resonance imaging (fMRI), with genetic data, such as single nucleotide polymorphisms (SNPs), to study the relationships between brain structure, function, and genetic variations (Abbas, Chi, & Chen, 2023; Scelsi et al., 2018; Smith et al., 2021). By integrating these different data types, researchers aim to explore the complex interactions between genes and brain function, gain insights into the underlying molecular mechanisms that contribute to human cognition and behavior, and understand how changes in these mechanisms may relate to neurological and psychiatric disorders (Li et al., 2020; Mahmud, Kaiser, McGinnity, & Hussain, 2021; Zhao et al., 2023). As a commonly used brain imaging technique, functional magnetic resonance imaging measures changes in blood oxygen levels to infer brain activity in different regions. Researchers can analyze fMRI data to investigate brain function in different cognitive states and disease conditions (Micheloyannis, Sakkalis, Vourkas, Stam, & Simos, 2005; Stam, van Walsum, & Micheloyannis, 2002). In recent years, there have been some brain imaging genetics approaches to reveal associations between brain function and genetic variation by integrating fMRI data and genetic data, thus providing a more comprehensive view of AD diagnosis (Bi et al., 2023; Golovanevsky, Eickhoff, & Singh, 2022; Sharma, Goel, Tanveer, Lin, & Murugan, 2023; Zhou et al., 2020). These methods can be categorized into two groups: correlation analysis-based and machine learning-based methods.

* Corresponding author.
*E-mail address:* weipeng1980@gmail.com (W. Peng).
[1] Equal Contribution.

https://doi.org/10.1016/j.neunet.2024.107020
Received 1 June 2024; Received in revised form 3 November 2024; Accepted 3 December 2024
Available online 20 December 2024

Correlation analysis-based methods focus on establishing links between brain regions and genes through regression and typical correlation analyses to extract discriminative features for AD diagnosis (Wei, Kong, & Wang, 2022). For example, Wang et al. (2012) proposed a method called G-SMuRFS to study the effects of genetic variants on brain structure and functions. It performs regression analysis to model the relationship between genetic variants (SNPs) and brain imaging features, aiming to identify the most relevant and informative genetic markers that contribute to AD-related imaging phenotypes. Greenlaw et al. (2017) used a multitask regression model to investigate the relationship between genetic variations and brain structure by integrating information from 486 single nucleotide polymorphisms (SNPs) with MRI measurements of brain volume and cortical thickness. Du et al. (2020) utilized sparse typical correlation analysis (SCCA) to establish associations between SNP data and MRI data, providing insights into how genetic variations may influence brain structure or function. Wang, Shao, Hao, Huang, and Zhang (2022) proposed a method called Deep Self-Reconstructing Sparse Typical Correlation Analysis (DS-SCCA) for analyzing the associations between genetic variants and fMRI data. Although traditional brain imaging genetics methods have bridged the gap between genetic variation and disease phenotypes in AD, they often assume a linear relationship between genetic variation and disease phenotypes in Alzheimer's disease and other neurological disorders. They are prone to ignoring the complex interactions between genetic molecules and disease phenotypes. In recent years, machine learning methods have successfully fused multi-modal and multi-omics data for AD diagnosis. For example, Bi, Hu, Wu and Wang (2020) obtained fusion features by calculating the correlation between a brain region and gene sequences. Then, a genetic evolutionary strategy and random forest (RF) were taken to integrate multiple classifiers to identify AD patients and discover some brain regions and genes significantly associated with AD. Batmanghelich, Dalca, Quon, Sabuncu, and Golland (2016) used a Bayesian framework to infer the posterior probability of correlations between image features and genetic variants and identify associations contributing to AD disease. In addition, several graph convolutional neural network (GCN)-based approaches have emerged in recent years approaches, which abstract multimodal data into graph structures with interconnections and learn new representations from their topologies (Gao, Shi, Shen, & Liu, 2021; Peng, Chen, & Dai, 2021; Peng, Tang, Dai, & Chen, 2022; Song, Mao, & Qian, 2021). For example, Bi, Zhou, et al. (2022) constructed a brain region-gene network using fMRI and SNP sequence data, where brain regions and genes were nodes and correlations were weighted for edges. A method called FAGCN was proposed to update the features of each node by aggregating information from neighbors and leveraging a full-gradient saliency graph mechanism to score and identify brain regions and genes associated with diseases. Shang et al. (2023) constructed a correlation map of brain imaging and genetic data of patients with mild cognitive impairments and ran a graph capsule convolutional network (GCCN) to learn their complex relationships. However, GCN-based methods still have some limitations (Jin, Zeng, Xia, Huang, & Liu, 2021). First, GCNs are primarily designed for processing graph-structured data. They are less suited for directly processing sequential data, such as time-series data from brain imaging. The sequences have temporal dependencies and order information recording the changes in brain regions over time. The position encoding strategy in the Transformer model can capture changes in brain regions over time and enhance the representation of brain regions, which is also essential for capturing long-distance dependencies of brain areas in time. Second, most of current GCN-based methods consider local effects between the genes and brain regions and ignore their long-range effects.

However, there are varying degrees of long-distance correlations between brain regions and genes to affect human cognition and behaviors. Studies have shown strong correlations between brain regions far apart in physical location (Alexander-Bloch, Giedd, & Bullmore, 2013). For example, gray matter volume in the hippocampus co-varies significantly with gray matter volume in other distant areas involved in memory systems, such as the amygdala and parahippocampal cortex, entorhinal cortex, and orbitofrontal cortex (Bohbot, Lerch, Thorndycraft, Iaria, & Zijdenbos, 2007). For genetic data, recent studies have shown that many known AD risk genes are under the long-range regulation of promoter-enhancer interactions (Meng et al., 2023). For example, Cursano et al. (2021) identified long-distance interactions between AD risk SNPs and the promoters of AD risk genes, such as BIN1, CR1, ARHGEF7, CEP72, MAPT and CRHR1, which may influence the transcription and activity of these genes in AD. On the other hand, multiple genes with long distances in the physical network can be co-regulated in the same brain region (Roshchupkin et al., 2016). Multiple distant brain regions can also be affected by a gene simultaneously, e.g., the frontal, parietal, temporal and occipital lobes and cerebellum are all associated with reduced levels of SNAP25 protein in AD patients (Furuya et al., 2012; Greber, Lubec, Cairns, & Fountoulakis, 1999). It is, therefore, necessary to design a method to mine the complex long-range interaction information between imaging phenotypes and genetic molecules (Arranz & De Strooper, 2019). In addition, fMRI data contain time-series information, which can capture changes in brain activity and help to understand the evolution of brain function over time (Hindriks et al., 2016). Researchers typically construct dynamic functional connectivity (dFC) to capture temporal changes in functional connectivity during fMRI acquisition (Hindriks et al., 2016; Kong et al., 2021). However, traditional dFC methods using sliding window-based correlations have several limitations, including increased data dimensionality, potentially redundant information, and sensitivity to window parameters. Transformer model (Vaswani et al., 2017) excels in capturing multilevel feature interactions between sequence data as well as mining long-range associations between data (Zhang, Han, Zhu, Sun, & Zhang, 2021). Moreover, the attention mechanism in Transformer can naturally consider feature contributions that are effective for downstream tasks, thereby providing intuitive interpretability for the prediction results (Hu, Wang, Jin, & Hou, 2023; Li, Zeng, Zhang, Wu, & Li, 2023; Qin, Liu, Guo, & Zhu, 2022; Xing et al., 2020). Some attention-based methods have been proposed for diagnosing AD. Most of them either adopt a self-attentive neural network to capture features from sMRI images for AD diagnosis Zhang et al. (2021) or Liu et al. (2023) use multiple cross-attention blocks to integrate information from different modalities between sMRI and clinical data to make AD predictions. However, few approaches efficiently combine imaging and genetic data and simultaneously consider the long-range and local interactions between both modalities.

To address the above challenges, we propose MCA-GCN, a Multi-stream Cross-Attention and Graph Convolutional Network-based classification method for AD patients. It first constructs a brain region-gene association network based on brain region fMRI time series and gene SNP data. Then it integrates the absolute and relative positions of the brain region time series to obtain a new brain region time series containing temporal information. To achieve a robust performance of our method, we partition it into three sub-modules: a Multi-view Long-Range Information Fusion (MLIF) Module with multi-stream cross-attention, a Local Information Aggregate (LIA) Module with graph convolutional network and a prediction module with the fully connected network. Moreover, we introduced a multi-stage feature scoring process for identifying brain regions and genes that are significantly associated with an AD diagnosis. This process breaks down predictions into multiple stages based on the sub-modules. It leverages different feature scoring strategies for these modules, generating score curves for essential genes and brain areas of diagnostic results. Compared with the existing methods, the contributions of our method are as follows:

- We introduce a learnable positional encoding method to incorporate absolute and relative temporal information at brain region nodes. This model can better capture changes in brain regions over time and enhance the representation of brain regions.

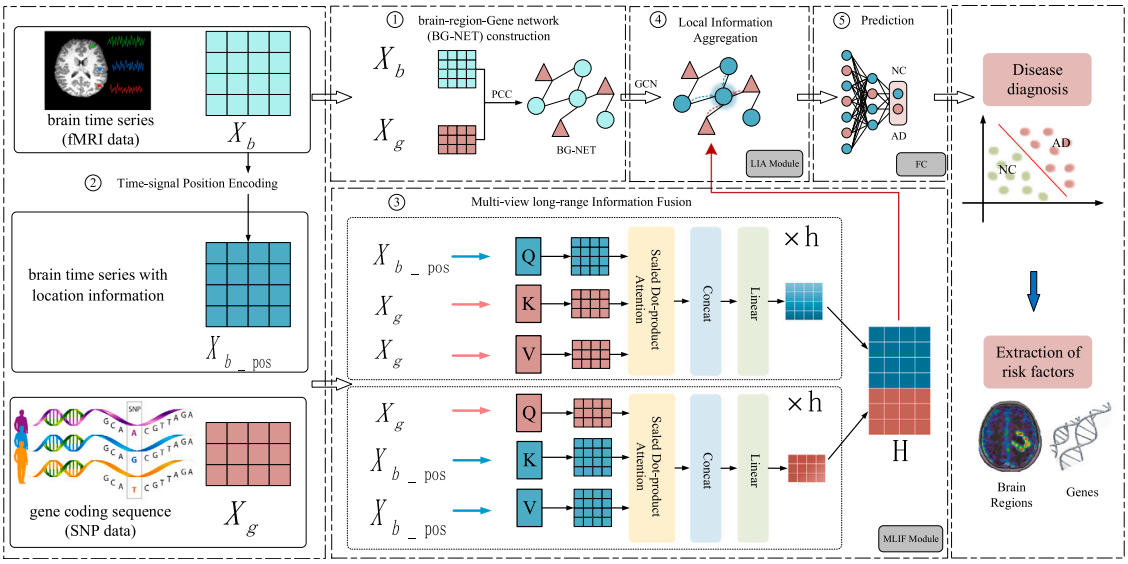


**Fig. 1.** The framework of MCA-GCN.

- We use a multi-stream cross-attention mechanism to learn brain region feature-based gene attention vectors and gene feature-based brain region attention vectors separately. This approach allows the model to learn long-range correlations between brain regions and genes from multiple perspectives and also consider the difference in genes in brain regions features.
- Learning brain region-gene associations both long-range and locally. A brain region-gene association network was constructed based on brain region fMRI time series and gene SNP data. Furthermore, a Graph Convolutional Network (GCN)-based local information transfer module is designed to learn local associations between brain regions and genes, providing a more comprehensive view of their relationships.
- MCA-GCN introduced a multi-stage feature scoring process that applies different feature scoring strategies to assigning weights to features (genes and brain areas) based on their importance or relevance to the classification task. By analyzing the score curves, the model identifies high-risk genes and brain regions that are associated with AD classification.

## 2. Data acquisition and pre-processing

### 2.1. Data acquisition

The Alzheimer's Disease Neuroimaging Initiative (ADNI) study is a longitudinal, multicenter research initiative focused on the early detection and tracking of Alzheimer's disease. The study includes participants with different cognitive statuses, including AD patients, cognitively normal controls (NC), and individuals with mild cognitive impairment (MCI). Mild cognitive impairment (MCI) is recognized as a potential precursor to AD and other types of dementia. According to the new criteria defined by ADNI, patients with MCI are categorized into two groups: early MCI (EMCI) and late MCI (LMCI). In this paper, 869 samples were obtained from ADNI, excluding samples disturbed by large head movements (exclusion criteria: maximum head movements of 2.0 mm and 2.0 degrees) (Jr et al., 2008). A final sample of 817 comprises 222 AD patients, 213 cognitively NC samples, 190 EMCI samples, and 192 LMCI samples. Among them, AD samples were from ADNI-2, ADNI-3, and ADNI-DOD. NC samples were from ADNI-3. EMCI and LMCI samples were from ADNI-GO, ADNI-2, and ADNI-3. The sample information is shown in Table 1, which includes which of the four types of samples came from which ADNI centers and their numbers.

**Table 1**
Sample information.

| Variables | AD | NC | EMCI | LMCI |
|---|---|---|---|---|
| Total sample number | 222 | 213 | 190 | 192 |
| ADNI-GO samples | / | / | 14 | 3 |
| ADNI-2 samples | 88 | / | 125 | 114 |
| ADNI-3 samples | 11 | 213 | 51 | 75 |
| ADNI-DOD samples | 123 | / | / | / |
| Age (mean ± std) | 71.83 ± 6.60 | 74.61 ± 7.86 | 73.64 ± 6.67 | 74.84 ± 8.00 |
| Gender (F/M) | 45/177 | 91/122 | 84/106 | 89/103 |

### 2.2. Data pre-processing

The MCA-GCN takes resting-state functional magnetic resonance imaging (rs-fMRI) data and single-nucleotide polymorphism (SNP) genetic data as input. To ensure the accuracy of the experiment, we took the following data preprocessing steps for rs-fMRI and genetic data.

We used DPARSF (Yan & Zang, 2010) to process the rs-fMRI data and in order to extract the time series of brain regions of interest (ROIs), the relevant parameters followed the standard settings in DPARSF (Yan, Wang, Zuo, & Zang, 2016) as follows: (1) Format Conversion: Converts rs-fMRI data in DICOM format to NIFTI format recognized by DPARSF. (2) Deletion of the first 10 time points: The instrument's magnetic field may be unstable and noisy during the first few time points. By deleting the first 10 time points for each subject, these potential confounding factors can be eliminated, ensuring that subsequent analyses are based on more stable and reliable data. (3) Time Layer Correction: Since brain scans are usually layered, there may be differences in scan times for the same brain region. The purpose of time layer correction is to correct these scans to the same point in time for more accurate time series analysis. (4) Head Motion Correction: With head motion correction, the image can be accurately corrected to the correct position, reducing the image position shift caused by the subject's head movement. (5) Spatial normalization: Normalizes brain imaging data from all subjects to match the echo planar imaging (EPI) template, ensuring that brain imaging data from different subjects can be aligned to the same standard space. (6) Image smoothing: Gaussian smoothing is performed on the image to improve the sex-to-noise ratio with smoothing parameters FWHM of [6, 6, 6]. Smoothing can help to reduce noise, highlight potential signals, as well as improve the overall quality of the image. (7) Filtering: By setting the filtering parameter to 0.01–0.08 Hz, low and high frequency noise can be removed, thus improving the quality of the image. (8) Covariate removal: eliminating some potential

interfering factors, including global signal, noise in gray matter white matter, etc. (9) Brain region time series extraction: using the AAL-116 template (Tzourio-Mazoyer, Landeau, Papathanassiou, Crivello, Etard, Delcroix, Mazoyer, & Joliot, 2002), the brain was divided into 116 brain regions aligned with the template, and the somatostatin blood oxygenation level-dependent (BOLD) signals of each brain region were calculated to obtain the functional average time series of the brain regions.

Quality control and pre-processing of SNP genetic data was performed using PLINK (Purcell et al., 2007) and MAGMA (de Leeuw, Mooij, Heskes, & Posthuma, 2015), with parameters set according to Marees et al. (2018), as follows: (1) Missing rate control: samples with excessive SNP missing rates and SNPs with excessive missing rates within the sample were filtered by a loose threshold (20%) and a strict threshold (2%), respectively. (2) Minimum allele frequency (MAF) control: in genomic association analysis, too low allele frequency may lead to unstable statistical effects, so setting a reasonable MAF threshold can help to improve the reliability and generalization of the results, in this paper, we set the MAF threshold to 0.05 to exclude the effect of rare variant loci. (3) Hardy-Weinberg equilibrium (HWE) test: The HWE test can be used to detect possible data errors and is an important quality control step in genomics research. Genotypes that do not conform to HWE may be affected by selection, mutation, or technical factors, and thus require quality control. In this paper, the threshold is set to 0.000001. (4) Linkage Disequilibrium (LD) pruning: removing highly correlated SNPs by calculating the LD levels among them can reduce genome-wide redundant information, avoid multiple comparison errors as well as reduce false positive results in genetic association analysis. In this paper, 200 SNPs were used as a sliding window to screen for SNPs with strong LD levels between them and other SNPs, based on a paired r2 threshold of 0.98 (Hinds, Kloek, Jen, Chen, & Frazer, 2006). (5) Mapping SNPs to genes: quality-controlled SNPs were mapped to the genes to which they belonged according to their physical location using MAGMA (reference human genome version as build-37 (Consortium, 2004)) to allow for further subsequent extraction of SNP-coding data from each sample. (6) Filtering genes using the Protein-Protein Interaction (PPI) network: these genes need to have edges in all 4 PPI networks (database-based PPI, experimental-based PPI, co-expression-based PPI, and text-mining-based PPI) downloaded from STRING (Szklarczyk et al., 2023). We verified the existence of dense network associations for these genes in the experimental part. In the end, we retained 42 genes to ensure that the dataset was sufficiently informative and relevant. (7) Gene coding: Finally, the gene SNPs data were coded into 0, 1, and 2 number sequences representing the pure common genotypes, heterozygous genotypes, and pure uncommon genotypes, respectively. For example, AA was coded as 0, AC as 1, CC as 2, and finally, each gene was represented as sequence data with a length of 90.

## 3. Methodology

### 3.1. Overview of MCA-GCN

Fig. 1 demonstrates the framework of MCA-GCN. It consists of five parts, 1. Brain Region-Gene Network (BG-NET) Construction: Brain region-gene association network BG-NET was constructed based on brain-region time series and gene SNP data. 2. Time-signal Position Encoding: the MCA-GCN introduces a learnable positional encoding method to integrate absolute and relative information of the brain region time series. 3. Multi-View Long-Range Information Fusion Module: Considering the differences between brain regions and genes, the MCA-GCN used the multi-stream cross-attention mechanisms to get the long-range correlations between brain regions and genes from the two perspectives of brain regions and genes, respectively. 4. Local Information Aggregate Module: the outputs in the multi-view long-range information fusion module are used as the initial features of brain regions and genes, and the graph convolutional neural network model is utilized to converge the local neighboring features in the brain region-gene network to learn the brain-region and gene feature representations. 5. Prediction: finally, we input the brain region and gene features into a fully-connected network to predict the disease type of AD.

### 3.2. BG-NETs network construction

The aim of this paper is to categorize AD patients by fusing rs-fMRI and genetic data, and to explore the brain regions and genes associated with AD. In order to correlate brain regions and genes, reduce the impact of inertia effects and accurately reflect steady-state neural activity, we retained the leaning time points and cropped the length of the brain region time series to the same length as the gene coding sequence (Fair et al., 2007; Fransson, 2005). That is, the number of brain region time points is 90. We constructed brain region-gene association networks (BG-NETs) by calculating the Pearson coefficients (PCC) between brain regions and genes. In mathematical form, BG-NETs are defined as $G = \{\mathcal{G}_1, \mathcal{G}_2, \ldots, \mathcal{G}_n\}$, where $n$ denotes the sample number, and $\mathcal{G}_i$ means the BG-NET of the $i$th sample. The labeling of the samples has been omitted in the rest of this section for ease of representation.

For any of the $\mathcal{G} = (\mathbf{A}, \mathbf{X})$, $\mathbf{X} \in \mathbb{R}^{N \times d}$ represents the embedding of $N_1$ brain regions and $N_2$ gene nodes, the $N = N_1 + N_2$. $\mathbf{X} = \begin{bmatrix} X_b \\ X_g \end{bmatrix}$, where $X_b \in \mathbb{R}^{N_1 \times d}$ denotes the brain-region time series, $N_1$ and $d$ represent the number of brain regions and time points respectively. $X_g \in \mathbb{R}^{N_2 \times d}$ denotes gene coding sequence, where $N_2$ and $d$ represent the number of genes selected after pre-processing and retained SNPs, and $A \in \mathbb{R}^{N \times N}$ means the association strength between nodes. The correlation strength $\mathbf{A}_{u,v}$ between node $u$ and node $v$ is measured by calculating the Pearson correlation coefficient between the sequence feature vectors of genes and brain regions. Some research work has proved the feasibility of this measurement (Bi, Wang, et al., 2022; Bi, Zhou, et al., 2022; Wang, Han, et al., 2022). The correlation calculation is as Eq. (1):

$$\mathbf{A}_{u,v} = \frac{d\sum_{t=1}^{d} x_u^t x_v^t - \sum_{t=1}^{d} x_u^t \sum_{t=1}^{d} x_v^t}{\sqrt{d\sum_{t=1}^{d} \left(x_u^t\right)^2 - \left(\sum_{t=1}^{d} x_u^t\right)^2} - \sqrt{d\sum_{k=1}^{d} \left(x_v^t\right)^2 - \left(\sum_{t=1}^{d} x_v^t\right)^2}} \tag{1}$$

Where $\mathbf{x}_u \in \mathbb{R}^d$ corresponds to the embedded of node $u$, and $\mathbf{x}_u^t$ represents the $t$th element of the embedded of node $u$.

### 3.3. Time signal position encoding

To better capture dynamic changes in brain regions over time, we added an additional positional encoding vector with the same dimension of the brain-region embeddings from the rs-fMRI data to reflect the position of each time point in the sequence (Dosovitskiy et al., 2020; Vaswani et al., 2017). Let $X_b \in \mathbb{R}^{N_1 \times d}$ be the original brain region embedding and $X_{b\_pos} \in \mathbb{R}^{N_1 \times d}$ be the new brain region embedding that adds the learned brain-region time point position information. $X_{b\_pos}$ can be calculated by Eq. (2). We proposed a novel position encoding approach that incorporates absolute and relative temporal information at brain region nodes by a learnable position encoding function $PE(\cdot)$ in Eq. (3).

$$X_{b\_pos} = X_b + PE\left(X_b\right) \tag{2}$$

$$PE\left(X_b\right) = F\left(X_b\right) + W_b \tag{3}$$

Where $F(\cdot)$ is an absolute position encoding function, and $W_b \in \mathbb{R}^{N_1 \times d}$ is a learnable temporal position embedding with the same dimension of $X_b$. The mathematical form of $F(\cdot)$ is shown below:

$$\begin{aligned} F(pos, 2i) &= sin\left(pos/10000^{2i/L}\right) \\ F(pos, 2i+1) &= cos\left(pos/10000^{2i/L}\right) \end{aligned} \tag{4}$$

Where $pos \in [0, d-1]$ denotes the time-point position of the $X_b$, and $L = N_1$ denotes the dimension of the time series vector, and $i \in [0, L/2)$ represents the $i$th component of the time series vector at position $pos$. It is worth noting that $X_{b\_pos}$ has the same dimension with $X_b$ and $PE(\cdot)$ position encoding function enables the model to learn the relative position easily. Since for any fixed offset $k$, $PE_{pos+k}$ can be expressed as a linear function of the $PE_{pos}$.

The positional encoding used in MCA-GCN combines both absolute and relative temporal information of brain region time series, which is crucial for capturing the dynamics of functional connectivity relevant to AD. The integration of absolute positional information allows the model to maintain a consistent reference point in the temporal dimension, ensuring that the sequential nature of the time series is preserved. This aspect is particularly important for tasks that require an understanding of the timing of events across different brain regions. On the other hand, relative positional information captures the relationships between different time points, enhancing the model's ability to identify patterns and changes that may signify early indicators of AD.

### 3.4. Multi-view long-range information fusion (MLIF)

We combined brain region time series ($X_{b\_pos}$) and gene coding sequences ($X_g$) as the input features of the multi-view long-range information fusion module. This module utilizes a multi-stream cross-attention mechanism to learn brain region feature-based gene attention vectors and gene feature-based brain region attention vectors separately (Ruan & Jin, 2022). The multi-stream cross-attention mechanism enables interaction and information transfer between two views of genes and brain regions to obtain their long-range information fusion, which captures a richer feature representation of brain regions and genes. We first introduce the self-attention (SA) mechanism, which serves as the foundation of the Multi-view Long-range Information Fusion (MLIF) module. Mathematically, the self-attention mechanism can be formulated as follows:

$$SA(Q, K, V) = softmax\left(\frac{QK^T}{\sqrt{d_k}}\right)V \tag{5}$$

where $Q$, $K$ and $V$ represent the query, key, and value, respectively. $\frac{1}{\sqrt{d_k}}$ is the scaling factor of the dot product attention. We achieve interaction and information transfer between the gene and brain region views by assigning different features to the query ($Q$), key ($K$), and value ($V$) matrices. Specifically, for brain region attention based on gene features, we assign $Q = X_{b\_pos}W_{q1}$, $K = X_gW_{k1}$ and $V = X_gW_{v1}$, allowing the model to focus on the brain regions while incorporating information from the gene features. Conversely, to obtain gene attention based on brain region features, we assign $Q = X_gW_{q2}$, $K = X_{b\_pos}W_{k2}$ and $V = X_{b\_pos}W_{v2}$, which enables the model to concentrate on the genes while leveraging information from the brain region features. Where $X_{b\_pos}$ denotes the brain features, $X_g$ denotes the gene features, and $W_q$, $W_k$, $W_v$ are the transformation matrices. Building upon this, we extend the framework to incorporate a multi-head attention ($MA$) mechanism, which enables the model to capture multiple attention representations simultaneously, as shown in Eq. (6) as follows:

$$MA(Q, K, V) = norm\left(concat\left(SA_1, SA_2, \dots, SA_h\right)W\right) \tag{6}$$

where $h$ is the number of heads, and $W$ is the learnable parameter matrix, and concat$(\cdot)$ denotes the concatenation operation, and norm$(\cdot)$ means the normalization function. $SA$ denotes the single-head attention, whose mathematical form is expressed as Eq. (5). Finally, we aggregate the outputs of each cross-attention head to obtain the final hidden features $H$, which is calculated by Eq. (7):

$$H = concat\left(MA\left(X_{b\_pos}, X_g, X_g\right), MA\left(X_g, X_{b\_pos}, X_{b\_pos}\right)\right) \tag{7}$$

where $H \in \mathbb{R}^{(N_1+N_2)\times c_1}$ are the feature matrices updated with multi-stream cross-attention, $c_1$ represents the feature dimension of multi-stream attention output, the $MA\left(X_{b\_pos}, X_g, X_g\right)$ and $MA\left(X_g, X_{b\_pos}, X_{b\_pos}\right)$ denote the brain region attention features based on gene features and the gene attention features based on brain region features, respectively, and the two cross-attention do not share the weights. $MA(\cdot)$ denotes the multi-head attention mechanism, which can be expressed as Eq. (6).

### 3.5. Local information aggregation (LIA)

In the MLIF module, long-range associations between multimodal data features are considered. To further consider local associations between features, an association matrix $\hat{A} \in \mathbb{R}^{N\times N}$ is formed by filtering out edges in the BG-NETs with low association strength (see Eq. (8)). Then, a graph neural network model is used to learn the local features in the nodes by passing information from neighboring nodes in the BG-NETs.

$$\hat{A}_{u,v} = \begin{cases} 1 & ,if\ \mathbf{A}_{u,v} > \lambda \\ 0 & ,otherwise \end{cases} \tag{8}$$

Where $\lambda$ denotes the association strength threshold. We tested the optimal value of $\lambda$ for different classification tasks in the experimental part. The mathematical form of GCN can be expressed as Eq. (9):

$$H^{(l+1)} = ReLU\left(\hat{D}^{-\frac{1}{2}}\hat{A}\hat{D}^{-\frac{1}{2}}H^{(l)}W^{(l)}\right) \tag{9}$$

Where $H^{(l)}$ denotes the node feature matrix of layer $l$, $W^{(l)} \in \mathbb{R}^{c_1\times c_2}$ represents the learnable filter of layer $l$, $c_2$ represents the feature dimension output by the convolutional layer, $\hat{A} = \hat{A} + I$ denotes the adjacency matrix $\hat{A}$ plus self-loop, and $\hat{D} \in \mathbb{R}^{N\times N}$ represents the degree matrix of $\hat{A}$. We take the long-range association features learned in the previous step ($H$, see Eq. (7)) as the node initial features of the GCN model, i.e: $H^{(0)} = H \in \mathbb{R}^{(N_1+N_2)\times c_1}$. Fusion features were obtained by aggregating long-range and local information from multimodal data through MLIF module and LIA module, respectively.

Finally, the fused features output from LIA module are input into the multilayer fully connected (FC) to obtain the predicted probability value $P$ of the sample. Binary cross-entropy loss was employed as the loss function for MCA-GCN training, and the loss function formula is shown in Eq. (10):

$$\mathcal{L}_{BCE}\left(\mathbf{y}_i, \mathbf{p}_i\right) = -\frac{1}{N}\sum_i \left[y_i \cdot log\left(p_i\right) + \left(1-y_i\right)\cdot log\left(1-p_i\right)\right] \tag{10}$$

Where $y_i$ denotes the actual label of the sample $i$, and $p_i$ is the predicted probability of the sample $i$, and $N$ is the number of samples.

### 3.6. Significant causal factor identification

In order to reveal the brain regions and genes that play an important role in the classification of AD and thus to identify the causative factors, we designed a multi-stage feature scoring process. For the three sequential modules of the model: MLIF module, LIA module and Prediction, MCA-GCN uses different feature scoring strategies to assign weights to features (genes and brain areas) based on their importance at different stages of the diagnostic process, aiming at the identification of causative factors.

Specifically, for the MLIF module, in each multi-stream attention, we first calculate the weight matrix for each head (Li et al., 2023). The weighted average of the weight matrices across all the heads yields the attention weight score for each brain region or gene, which represents the importance of different brain regions or genes for the given prediction task. The attention weight score can be calculated by Eq. (11):

$$\alpha = \frac{1}{H_1}\sum_{h=1}^{H_1}\frac{Q^h\left(K^h\right)^T}{\sqrt{d_h}} \tag{11}$$

Where $\alpha$ is the weight matrix, and $h$ is the number of heads. When $Q = X_{b\_pos}W_{q1}$, $K = X_gW_{k1}$, $\alpha_g \in \mathbb{R}^{N_1\times N_2}$ in Eq. (11) denotes the weight matrix of brain regions based on genetic features. Similarly, when $Q = X_gW_{q2}$, $K = X_{b\_pos}W_{k2}$, $\alpha_b \in \mathbb{R}^{N_2\times N_1}$ denotes the gene weight matrix based on brain region features.

Next, the weighted score vectors $Z^b \in \mathbb{R}^{N_1\times 1}$, $Z^g \in \mathbb{R}^{N_2\times 1}$ of brain regions and genes are obtained according to Eqs. (12) and (13).

$$Z^b_{(1)i} = \sum_{j=1}^{d} \left(\alpha_b \cdot X_{b\_pos}\right)_{ij} \tag{12}$$

$$Z^g_{(1)i} = \sum_{j=1}^{d} \left(\alpha_g \cdot X_g\right)_{ij} \tag{13}$$

Among them, $(\cdot)_{ij}$ represents the $j$th score of the $i$th brain region or gene feature. Finally, the score $Z_{(1)} = \begin{bmatrix} Z^b_{(1)} \\ Z^g_{(1)} \end{bmatrix} \in \mathbb{R}^{(N_1+N_2)\times 1}$ of the feature in the MLIF module is obtained.

For the LIA module, the learnable filter $W^{(l)}$in Eq. (9) represents the contribution of each feature to classification (Bi et al., 2023). The parameters in the filter are analyzed through Eq. (14), and brain regions and genes related to AD are scored to obtain a score $Z_{(2)} \in \mathbb{R}^{(N_1+N_2)\times 1}$.

$$Z_{(2)i} = \sum_{j=1}^{c_2} \left(H^{(l)} \cdot W^{(l)}\right)_{ij} \tag{14}$$

SHapley Additive exPlanations (SHAP) (Lundberg & Lee, 2017) is a unified framework for interpreting machine learning models. The core idea of SHAP value is derived from the concept of Shapley value in cooperative game theory, which aims to measure the contribution of each feature to the overall model prediction by considering the interaction between features. Inspired by existing research, we utilize SHAP to associate the prediction results of a fully connected classifier (FC) with the generated features (Qiu et al., 2022). Analyzing the SHAP values yields the feature score $Z_{(3)} \in \mathbb{R}^{(N_1+N_2)\times 1}$ of the prediction stage:

$$\phi_i(f) = \sum_{S\subseteq\{1,2,\ldots,q\}\setminus\{i\}} \frac{|S|!(q-|S|-1)!}{q!}[f(S\cup\{i\}) - f(S)] \tag{15}$$

$$Z_{(3)i} = \sum_{j=1}^{c_2} \phi_{ij} \tag{16}$$

where $\phi_i(f)$ is the SHAP value of feature $i$, $f$ is the model, $S$ is the subset of features, $q$ is the total number of features, $|S|$ is the size of the subset of features, and $f(S\cup\{i\}) - f(S)$ calculates the difference between the predicted outputs of the samples that include feature $i$ and those without the features.

Finally, considering the average contribution of each feature over all sample, the feature score $Z \in \mathbb{R}^{(N_1+N_2)\times 1}$ of the model is calculated by Eq. (17):

$$Z = \frac{1}{N}\left(Z_{(1)} + Z_{(2)} + Z_{(3)}\right) \tag{17}$$

Where $N$ represents the number of samples. The features (i.e., genes and brain areas)that have the higher $Z$ score are essential in AD diagnosis. Fig. 2 shows an example of how the brain regions and gene features are scored and gradually summed up at each stage to the AD classification task. For example, the highest scoring brain region, PHG.R ($Z$ = 23.516), scored fourth in MLIF module ($Z_{(1)}$ = 8.404) but ended up with the highest final score as the next two scores ($Z_{(2)}$ = 12.854, $Z_{(3)}$ = 2.258) were accumulated. The gene CDH4 ($Z$ = 10.835), which scored fourth in LIA module ($Z_{(1)}$ = 5.662, $Z_{(2)}$ = 5.148), became ninth in the final score because of the low scores ($Z_{(3)}$ = 0.025) accumulated at the end.

### 3.7. Computation complexity analysis

Given the length of the brain region time series is $N_1$ (number of brain regions) and the length of the gene coding sequence is $N_2$ (number of genes), the time complexity of the cross-attention is $O(N_1\times N_2)$, because there are two cross-attention layers, the time complexity of the MLIF module is $O(2\times N_1\times N_2)$, where N1 > N2. For the LIA module, there are $N(N = N_1 + N_2)$ nodes and $E$ edges, then for each node, the characteristics of its neighboring nodes need to be considered, so the time complexity is $O(N\times E)$. The time complexity of the fully connected layer is $O(N_\alpha \times M)$, where $N_\alpha$ is the fully connected input dimension and $M$ is the output dimension. So the total time complexity of the model is $O(2\times N_1\times N_2) + O(N\times E) + O(N_\alpha\times M)$.

## 4. Experiment and result analysis

We evaluated the MCA-GCN model on four independent classification tasks, AD diagnosis (NC vs AD), early MCI diagnosis (NC vs LMCI), AD and its early subtype distinction (LMCI vs AD), and MCI two subtype distinction (EMCI vs LMCI). At the same time, the performance of each method when using multi-modal data and unimodal data was compared, including using only fMRI data, using only genetic data, and using both fMRI data and genetic data (Dual). We compared the performance of the MCA-GCN model when using both fMRI and genetic data (Dual) and unimodal data (fMRI only, genetic only). In each independent classification task, we randomly split all the data into a training set and a test set, where 80% is used for training and the remaining 20% is used for testing. We then used five-fold cross-validation on the training set to optimize the hyperparameters of the MCA-GCN models, and the independent test set was used for the final evaluation of the models' performance. All models were tuned to their respective hyperparameters to ensure the fairness of the experiments.

In addition, to analyze the contribution of each module in MCA-GCN, we conducted ablation experiments by removing different components of the model and evaluating the performance. Then, we also compared our proposed location coding method with several mainstream location coding methods to validate its effectiveness. Then, we thoroughly analyzed the experimental results to verify the reliability of the results. Finally, we compared our model with state-of-the-art baseline methods.

### 4.1. Evaluation indicators

The classification performance measures used in this work include: accuracy (ACC), sensitivity (SEN), specificity (SPE), f1 score (F1), Matthews correlation coefficient (MCC), and area under the ROC curve (AUC). These metrics were calculated as follows:

$$ACC = \frac{TP+TN}{TP+FP+TN+FN} \tag{18}$$

$$SEN = \frac{TP}{TP+FN} \tag{19}$$

$$SPE = \frac{TN}{TN+FP} \tag{20}$$

$$F1 = \frac{2*TP}{2*TP+FP+FN} \tag{21}$$

$$MCC = \frac{TP*TN - FP*FN}{\sqrt{(TP+FP)*(TP+FN)*(TN+FP)*(TN+FN)}} \tag{22}$$

$$\text{AUC} = \int_{-\infty}^{\infty} FPR(x)dTPR(x) \tag{23}$$

where $TP$, $FP$, $TN$, and $FN$ denote true positive, false positive, true negative, and false negative, respectively. $FPR = \frac{FP}{TN+FP}$ represents the false positive rate, and $TPR = \frac{TP}{TP+FN}$ means the true positive rate.

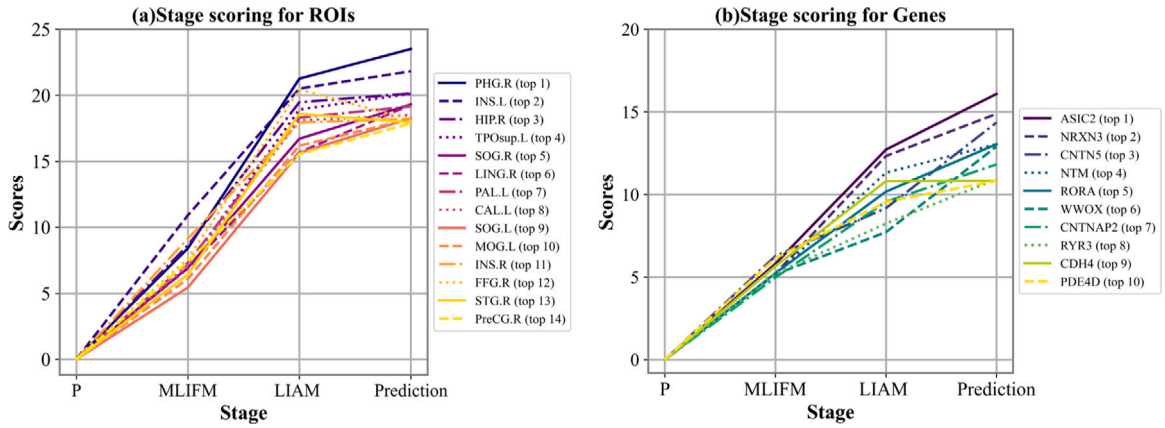


**Fig. 2.** Scoring curves of brain areas and genes across different stages of the model. **P**: the initial state of the model, all feature scores are initialized to 0. The scores at each stage include the scores from all previous stages.

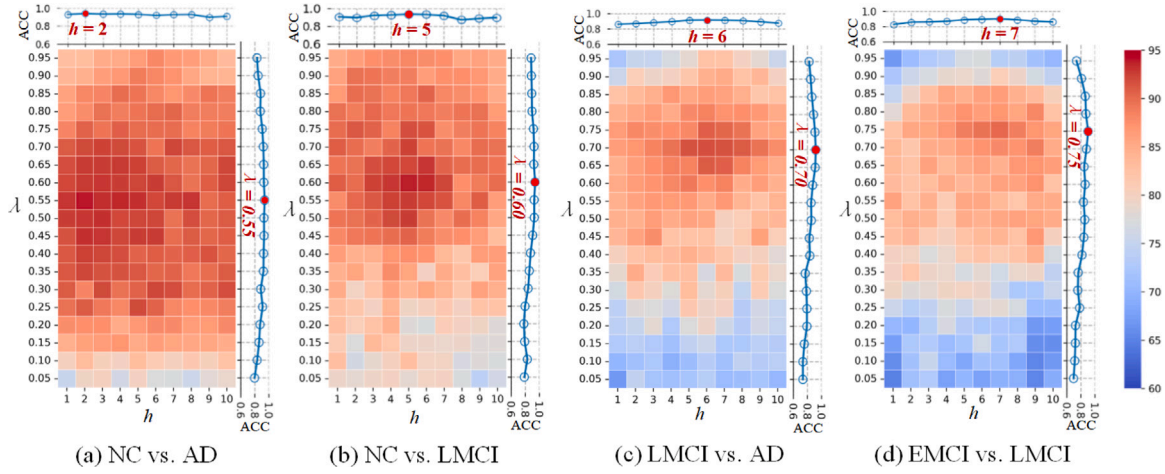


**Fig. 3.** Parametric sensitivity experiments for correlation strength threshold $\lambda$ and attention head count $h$.

### 4.2. Optimization parameters

The parameter $\lambda$ denotes the association strength threshold, controlling the correlation pattern between brain regions and genes. The parameter $h$ determines the number of heads for the multi-head attention mechanism. To analyze the impact of the two parameters on the classification performance, we set various values of the two parameters from the range $\lambda = \{0.05, 0.1, 0.15, \ldots, 0.95\}$, $h = \{1, 2, 3, \ldots, 10\}$ in the cross-validation, respectively. Fig. 3 demonstrates the results of the parameter sensitivity experiments under four classification tasks. We observed that the association strength threshold $\lambda$ the results, suggesting that the correlation pattern between brain regions and genes can improve the model performance, the optimal range for $\lambda$ is $[0.55, 0.75]$. In this paper, the optimal values $\lambda$ in the four tasks were 0.55 (NC vs AD), 0.60 (NC vs LMCI), 0.70 (LMCI vs AD), and 0.75 (EMCI vs LMCI). For another parameter $h$, the multiple attention mechanism allows the MCA-GCN to jointly attend to the diversity of interaction patterns from different representation subspaces. In most cases, a moderate increase in head numbers improves the model's classification accuracy. However, a continued increase in the head numbers beyond an optimal value leads to decreased model performance, which suggests that adding too many heads may lead to overfitting or inefficiencies in capturing relevant information. The optimal range for $h$ is $[2, 7]$. The optimal values $h$ taken in the four tasks were 2 (NC vs AD), 5 (NC vs LMCI), 6 (LMCI vs AD), and 7 (EMCI vs LMCI).

### 4.3. Analyzing MCA-GCN candidate genes

MCA-GCN selected 42 candidate genes to learn discriminative features for Alzheimer's diagnosis based on the length of the gene SNPs and whether they appeared in the PPI. To further analyze the effectiveness of these candidate genes for AD classification, we used Metascape (Zhou et al., 2019) to perform the KEGG pathway and the GO function enrichment analysis on the 42 candidate genes (see Fig. 4). We observed that these genes have axon development, neuron identification, and trans-synaptic signaling functions, and they were enriched in signaling pathways such as disruption of postsynaptic signaling and hippocampal signaling regulation. We further analyzed these 42 genes and found 900 edges between them, with an average degree of 19, a maximum degree of 36 (appearing in gene PTPRD), and an average aggregation coefficient(The weight of the edge in the network) of 45.50, constituting a denser subnetwork (Fig. 5). These genes interact with each other and perform functions closely related to the development of brain diseases such as AD, thus validating the reliability of our method for selecting candidate genes.

### 4.4. Comparative experiments with ML and DL methods

We conducted comparative experiments between several popular machine learning (ML) methods and deep learning (DL) methods, including Random Forest (RF), Support Vector Machine (SVM) (Tanveer et al., 2020), Convolutional Neural Network (CNN), Transformer, Graph

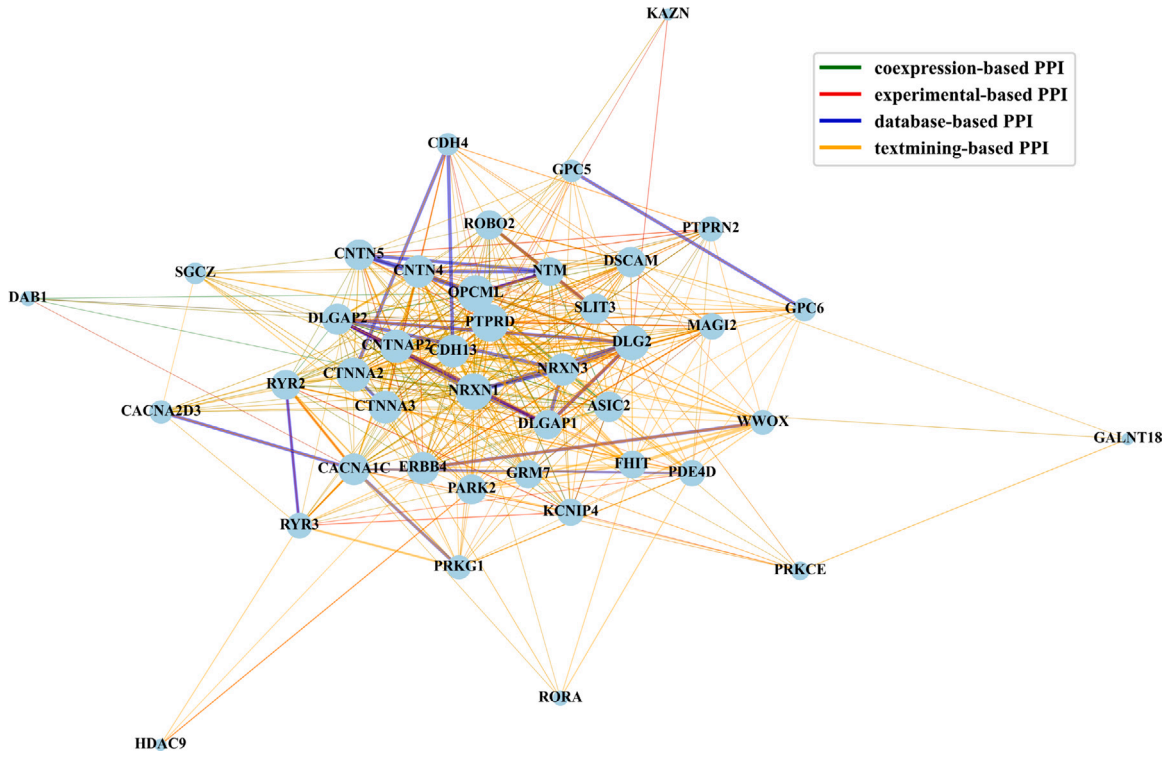


**Fig. 4.** Results of GO and KEGG enrichment analysis of 42 candidate genes by Metascape.

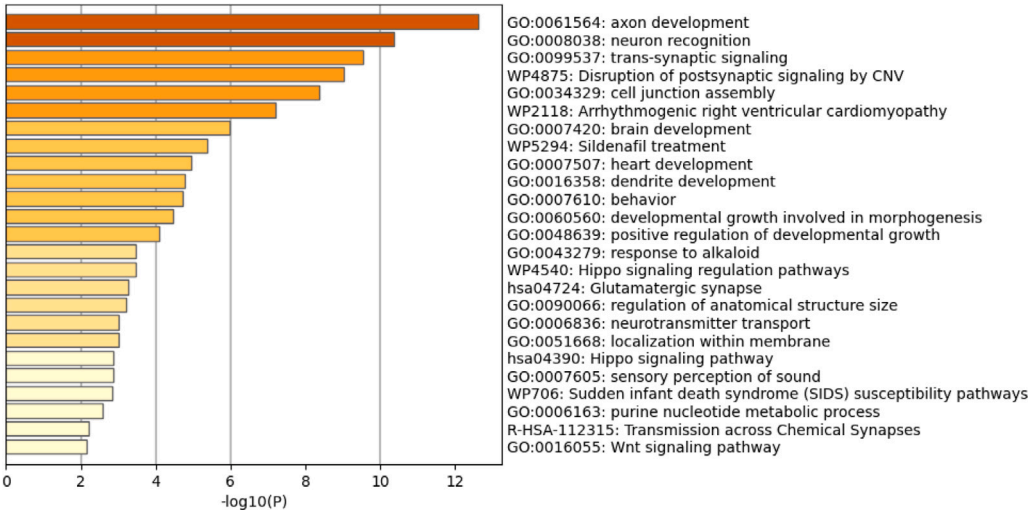


**Fig. 5.** 42 candidate genes between the four PPI networks. The thickness of the line represents the weight of the relationship.

Convolutional Network (GCN) and three advanced fMRI analysis models: BrainNetworkTransformer (BNT) (Kan et al., 2022), Community-Aware Transformer (Com-BNTF) (Bannadabhavi, Lee, Deng, Ying, & Li, 2023) and BolT (Bedel, Sivgin, Dalmaz, Dar, & Çukur, 2023). In addition, we compare two variants of MCA-GCN, namely EX-GCN and MA-GCN. EX-GCN exchanges the order of the Multi-view Long-range Information Fusion (MLIF) module and Local Information Aggregation (LIA) module, and it first splices brain region time series and gene coding sequences as input features for GCN models. Then, it uses a single-stream multi-head attention mechanism to learn gene features and brain region features from the output features of the GCN. MA-GCN differs from MCA-GCN by transforming MLIF module from a multi-stream multi-head attention structure to a single-stream multi-head attention structure, with the same module order as MCA-GCN. Four classification tasks related to AD and MCI were compared using brain region time series and gene coding sequences as input. When utilizing unimodal data, we directly use the corresponding input fMRI data or gene data for machine learning models such as Random Forest (RF), Support Vector Machine (SVM) and deep learning models such as Convolutional Neural Network (CNN), and Transformer. For GCN-based methods, including GCN, MCA-GCN, and its variants EX-GCN and MA-GCN, we include fMRI data or gene data along with the adjacency matrix, which is constructed using the Pearson correlation coefficient (PCC) and a thresholding procedure to filter weak correlations. When employing multimodal data, we concatenate fMRI data and gene data as input for RF, SVM, CNN, and Transformer, while GCN-based methods also incorporate the adjacency matrix of the concatenated data. For the three advanced fMRI analysis models BNT, Com-BNTF, and BolT, the time series of every brain regions were employed as the input.

The results when brain regions are extracted using the AAL-116 template are detailed in Tables 2 and 3. To validate the robustness and effectiveness of our model, we further expanded our analysis. We reprocessed all resting-state fMRI (rs-fMRI) data to extract 400 brain regions using the Schaefer-400 atlas (Ewers et al., 2021). Apart from the differences in the atlas used, the remaining fMRI data processing procedures remain consistent with those employed when using the AAL atlas, the time series data of 400 ROIs were extracted. The results are presented in Tables 4 and 5. When using the AAL-116 template to divide 116 brain regions, the MCA-GCN method that fuses fMRI and SNP data achieves the optimal classification performance among the six evaluation metrics under three classification tasks (NC vs LMCI, LMCI vs AD, EMCI vs LMCI). Its performance was slightly inferior to that of BNT and Com-BNTF while higher than BolT in the AD vs NC classification task. When using the Schaefer-400 template as the brain region atlas, the MCA-GCN method that fuses fMRI and SNP data controls the best classification performance in the AD vs NC task and has the second-best performance under three classification tasks (NC vs LMCI, LMCI vs AD, EMCI vs LMCI). Its performance was slightly inferior to itself when only using gene data. The results indicate that incorporating the association information between brain regions and genes is beneficial for predictive performance but also highlight the effectiveness of the proposed multi-modal and multi-stream attention mechanism in MCA-GCN, which enables the model to extract relevant information from both global and local associations between brain regions and genes.

Compared with three advanced fMRI analysis models, BNT, Com-BNTF, and BolT, MCA-GCN only using fMRI data was inferior to BNT and Com-BNTF while is comparable with BolT in the AD vs NC and NC vs LMCI task under both AAL-116 and Schaefer-400 brain region atlas. In the following two tasks (LMCI vs AD, EMCI vs LMCI), the performance gap between MCA-GCN only using fMRI data and the three advanced fMRI analysis models gradually diminished. It performs better than Com-BNTF and BolT while being slightly worse than BNT in the LMCI vs AD task and performing better than the three methods in the EMCI vs LMCI task under the two brain atlas.

We also observed that all methods performed lower under the Schaefer-400 Atlas than under the AAL-116 Atlas. The Schaefer 400 atlas provides 400 distinct brain regions parcellation, while the AAL-116 Atlas provides 116 ROIs. The finer granularity of the Schaefer 400 Atlas may introduce more noise due to the smaller size of each ROI, leading to a decreased signal-to-noise ratio as these smaller regions might capture less coherent neural activity. Additionally, the integration of gene and imaging data may be more challenging with the Schaefer 400-Atlas due to the complexity of interactions among a larger set of brain regions, which can introduce noisy interactions between brain regions and between brain regions and genes. We also notice that under the Schaefer-400 Atlas, MCA-GCN only using gene data performs better than that integrating gene data and fMRI data in three classification tasks(NC vs LMCI, LMCI vs AD, EMCI vs LMCI).

The performance change of all methods under the two brain region atlas highlights the noisiness of the fMRI data, which is expected to develop methods to effectively extract fMRI features for AD diagnosis. BNT and Com-BNTF exhibit impressive performance in AD vs NC and NC vs LMCI classification tasks, which may be because they take advantage of the community structure of normal brains. However, our MCA-GCN model considers global and local associations between brain regions, so it surpassed the three advanced fRMI data analysis models in LMCI vs AD and EMCI vs LMCI tasks. MCA-GCN outperformed its two variants, EX-GCN and MA-GCN, demonstrating that the specific order and combination of long-range information fusion and local information transfer modules in MCA-GCN contribute to its superior performance. Future work should still focus on designing methods to learn fMRI features effectively.

### 4.5. Ablation experiments

To investigate the contribution of each module in MCA-GCN, we conducted ablation experiments by removing the Multi-view long-range information fusion (MLIF) module, local information transfer (LIA) module, and location coding in MCA-GCN, respectively, and evaluating the performance. Tables 6 and 7 show that (1) increasing positional encoding of time series in brain regions is beneficial to improve the model's ability to classify AD diseases. (2) local information aggregation significantly affects the performance of the classification, suggesting that local association information between brain regions and genes is closely related to disease development. MCA-GCN can take advantage of long-range and local information aggregation and achieve more significant performance improvement. (3) genetic and fMRI data fusion improves performance compared to single-modality data. Genetic data demonstrated an advantage in most tasks compared to fMRI data, suggesting that genetic mutations may more directly contribute to brain disorders. The advantage of Dual is that for AD, it can provide a complete chain of evidence from micro genetic molecules to the macro brain level.

### 4.6. Comparison of positional encoding methods

This section compares the proposed positional encoding method with four popular positional encoding methods. The four positional encoding methods are:

- Transformer (Vaswani et al., 2017): uses sine and cosine functions to encode positional information in an input sequence.
- ViT (Dosovitskiy et al., 2020): adds a trainable position coding matrix to represent the position information.
- Swin-T (Liu et al., 2021): divides the input sequence into regions and represents the positional information by learning the relative positional biases between the regions.
- MAE (He et al., 2022): encodes positional information using sine and cosine functions in two dimensions of the input sequence.

The positional encoding used in MCA-GCN combines absolute and relative temporal information of brain-region time series. Therefore, Transformer and ViT can be considered as the ablation of the MCA-GCN positional encoding method. The experimental results in Fig. 6 show that the positional encoding used by Transformer enables the model to perform better AD disease classification. ViT also effectively extracts the positional information of the time series of functional signals in brain regions. The MCA-GCN positional encoding combines Transformer and ViT by incorporating the absolute positional information of temporal coding and the learned time-varying information, thus effectively encoding brain region features related to AD diseases.

### 4.7. Comparison with state-of-the-art methods

To validate the effectiveness of our method, we compared MCA-GCN with other state-of-the-art methods for Alzheimer's disease diagnosis. These state-of-the-art methods include the approaches using unimodal (Bi et al., 2023; Gan et al., 2021; Xing et al., 2020) and multimodal data (Bi et al., 2023; Bi, Wang, et al., 2022; Bi, Zhou, et al., 2022; Tian et al., 2023; Wang, Li, Li, & Lu, 2022; Zhou et al., 2020)and the approaches with attention mechanisms (Qin et al., 2022; Tian et al., 2023; Wang, Li, et al., 2022; Xing et al., 2020) or without attention mechanisms (Bi et al., 2023; Bi, Wang, et al., 2022; Bi, Zhou, et al., 2022; Gan et al., 2021; Zhou et al., 2020). As shown in Table 8, we found that MCA-GCN achieved the highest ACC and AUC in most classification tasks compared to existing state-of-the-art methods. Additionally, we also listed the input formats of fMRI data used by each method in the Table. These results indicate that MCA-GCN can effectively fuse information from different sources and achieve superior performance by combining a multi-stream attentional mechanism with graph convolutional networks.

**Table 2**
Performance comparison of different methods using AAL-116 atlas for time series extraction (NC vs AD and NC vs LMCI).

| Data | Method | NC versus AD | | | | | | NC versus LMCI | | | | | |
|---|---|---|---|---|---|---|---|---|---|---|---|---|---|
| | | ACC(std.) | SEN(std.) | SPE(std.) | F1(std.) | MCC(std.) | AUC(std.) | ACC(std.) | SEN(std.) | SPE(std.) | F1(std.) | MCC(std.) | AUC(std.) |
| fMRI | RF | 54.85(1.06)* | 54.20(0.65)* | 56.19(0.49)* | 55.35(0.63)* | 22.08(0.81)* | 55.93(0.47)* | 52.55(0.37)* | 56.99(1.24)* | 50.96(0.69)* | 52.44(0.67)* | 19.99(0.89)* | 52.37(0.63)* |
| | SVM | 56.96(0.69)* | 57.51(0.85)* | 57.05(0.66)* | 57.33(0.77)* | 20.96(0.81)* | 56.50(0.81)* | 55.67(0.85)* | 59.73(0.89)* | 47.94(1.16)* | 52.75(0.62)* | 25.09(0.91)* | 58.71(1.54)* |
| | CNN | 62.32(1.19)* | 63.37(0.77)* | 62.00(0.47)* | 62.70(1.35)* | 27.90(0.73)* | 62.49(1.07)* | 60.07(1.00)* | 61.17(1.03)* | 59.37(0.55)* | 59.71(0.65)* | 27.31(0.76)* | 60.07(0.62)* |
| | Transformer | 70.02(0.54)* | 69.37(0.5)* | 70.55(1.04)* | 70.09(0.78)* | 33.27(0.76)* | 70.46(1.43)* | 66.01(0.82)* | 70.37(0.34)* | 64.62(0.85)* | 66.18(0.62)* | 30.65(0.42)* | 65.84(1.01)* |
| | GCN | 67.99(1.00)* | 67.75(0.95)* | 68.99(0.74)* | 68.38(0.67)* | 29.36(0.79)* | 68.17(0.80)* | 64.55(0.46)* | 69.39(0.54)* | 59.60(0.84)* | 63.66(0.87)* | 27.61(0.58)* | 64.30(0.68)* |
| | EX-GCN | 76.19(0.50)* | 77.42(1.29)* | 75.21(1.35)* | 75.75(0.66)* | 44.88(0.77)* | 76.20(0.64)* | 73.32(0.33)* | 76.98(0.76)* | 64.90(0.99)* | 69.27(0.93)* | 43.73(1.36)* | 72.83(1.09)* |
| | MA-GCN | 85.10(0.31)* | 83.83(1.01) | 86.69(1.69) | 85.60(1.29) | 62.06(0.78)* | 85.14(0.62)* | 84.18(0.57)* | 84.49(0.69)* | 82.25(1.87) | 83.77(1.26) | 60.18(0.47)* | 84.14(1.06)* |
| | BNT | 94.94(1.74) | 93.18(1.61) | **96.74**(2.65) | 94.91(1.72) | 89.97(3.51) | 94.96(1.75) | 86.42(3.60) | 78.95(4.93) | **93.02**(8.22) | 84.58(3.50) | 73.60(7.44) | 85.99(3.39) |
| | Com-BNTF | **95.17**(2.21) | **93.63**(1.02) | 96.74(3.89) | **95.17**(2.12) | **90.44**(4.48) | 95.19(2.23) | **87.41**(1.61) | **90.53**(1.45) | 84.65(4.22) | **87.12**(1.26) | **75.14**(2.79) | 87.59(1.44) |
| | BolT | 85.29(5.88) | 81.36(14.5) | 89.30(10.5) | 84.37(7.77) | 72.22(10.4) | **95.42**(2.25) | 81.73(13.0) | 74.74(33.4) | 87.91(9.21) | 74.78(27.1) | 65.46(22.5) | **93.64**(2.16) |
| | MCA-GCN | 86.22(0.53) | 84.37(0.95) | 88.20(0.81) | 86.39(1.08) | 65.39(0.56) | 86.17(0.54) | 85.67(0.45) | 87.08(0.70) | 83.15(0.95) | 84.25(0.76) | 61.47(0.76) | 85.50(0.85) |
| Gene | RF | 61.69(1.55)* | 62.93(0.69)* | 61.31(1.83)* | 61.96(1.77)* | 29.01(0.64)* | 68.64(0.89)* | 59.86(0.88)* | 60.82(0.80)* | 59.34(2.44)* | 58.67(1.28)* | 28.74(0.94)* | 67.11(0.47)* |
| | SVM | 65.89(0.45)* | 59.71(0.78)* | 71.11(1.06)* | 65.51(1.16)* | 34.64(0.41)* | 68.54(0.58)* | 63.06(1.09)* | 69.64(1.19)* | 53.98(0.78)* | 61.23(0.82)* | 31.39(1.68)* | 66.49(0.43)* |
| | CNN | 68.61(0.37)* | 67.90(0.84)* | 69.15(1.72)* | 68.86(0.97)* | 39.99(0.41)* | 68.83(0.48)* | 67.56(0.91)* | 70.45(0.38)* | 64.81(0.88)* | 66.51(1.51)* | 35.96(2.24)* | 67.44(0.75)* |
| | Transformer | 70.38(0.71)* | 69.33(0.71)* | 70.8(1.23)* | 71.34(0.38)* | 41.31(1.30)* | 70.61(1.17)* | 68.64(1.35)* | 73.69(1.26)* | 64.37(0.80)* | 70.22(0.67)* | 35.64(1.38)* | 69.34(0.82)* |
| | GCN | 73.77(0.74)* | 73.07(1.20)* | 75.28(1.61)* | 74.15(0.71)* | 45.44(0.87)* | 73.98(0.52)* | 70.83(0.82)* | 74.06(0.88)* | 70.69(1.00)* | 69.70(2.29)* | 41.25(1.25)* | 70.68(0.80)* |
| | EX-GCN | 82.57(0.29)* | 80.03(0.64)* | 85.22(1.32)* | 83.36(0.74)* | 58.73(0.42)* | 82.50(0.70)* | 80.17(0.81)* | 81.35(0.94)* | 79.33(0.79)* | 79.69(0.63)* | 57.49(1.32)* | 80.22(1.06)* |
| | MA-GCN | 86.48(0.48)* | 83.94(1.05)* | 88.14(1.07) | 87.14(0.80)* | 64.26(0.58)* | 86.42(0.55)* | 84.93(0.75)* | 85.30(0.95)* | 84.72(0.67)* | 84.39(1.22)* | 61.36(1.44)* | 84.89(1.03)* |
| | MCA-GCN | **87.34**(0.60) | **85.84**(0.99) | **89.05**(1.34) | **87.86**(1.08) | **67.14**(0.70) | **87.32**(0.43) | **86.90**(0.69) | **92.34**(0.50) | **85.13**(1.37) | **85.44**(1.05) | **62.08**(0.93) | **86.61**(1.24) |
| Dual | RF | 62.57(0.61)* | 63.61(1.29)* | 62.35(1.04)* | 62.99(0.90)* | 36.28(1.26)* | 66.12(0.85)* | 62.62(0.95)* | 63.76(0.80)* | 61.57(1.37)* | 62.04(0.70)* | 34.80(0.82)* | 65.03(0.90)* |
| | SVM | 65.90(0.16)* | 64.70(0.87)* | 66.10(1.03)* | 68.51(1.36)* | 39.64(0.85)* | 73.53(0.64)* | 67.93(0.35)* | 74.22(1.01)* | 61.14(1.12)* | 66.16(0.90)* | 36.96(1.04)* | 71.61(0.90)* |
| | CNN | 75.66(0.29)* | 72.01(0.74)* | 78.30(0.78)* | 75.56(0.81)* | 48.80(0.49)* | 75.96(0.41)* | 73.42(0.74)* | 76.38(0.73)* | 70.29(0.91)* | 72.39(1.25)* | 43.22(0.83)* | 73.13(0.58)* |
| | Transformer | 76.94(1.14)* | 72.3(0.83)* | 81.66(0.67)* | 77.06(0.88)* | 76.93(0.51)* | 51.46(0.87)* | 74.65(0.67)* | 77.97(1.19)* | 70.33(1.36)* | 73.48(0.75)* | 42.69(1.01)* | 74.53(0.68)* |
| | GCN | 80.47(0.29)* | 80.03(0.64)* | 81.74(1.32)* | 80.91(0.74)* | 53.89(0.42)* | 80.68(0.70)* | 77.66(0.81)* | 82.70(0.94)* | 72.26(0.79)* | 76.46(0.63)* | 48.81(1.32)* | 77.28(1.06)* |
| | EX-GCN | 85.91(0.69)* | 84.83(1.19)* | 87.43(1.62)* | 85.43(1.28)* | 64.72(0.42)* | 86.01(0.61)* | 82.95(0.90)* | 87.68(0.59)* | 82.10(0.89)* | 83.98(1.40)* | 64.66(0.55)* | 82.85(0.64)* |
| | MA-GCN | 92.53(0.92) | 90.72(0.68)* | 93.62(1.27) | 92.40(1.56)* | 80.58(0.81)* | 92.36(0.53)* | 90.10(0.46)* | 92.60(0.38)* | 87.42(0.80)* | 89.44(0.94)* | 74.27(0.83)* | 89.95(0.80)* |
| | MCA-GCN | **93.27**(0.59) | **92.98**(1.04) | **93.89**(1.16) | **93.12**(0.97) | **80.59**(0.91) | **92.55**(0.65) | **91.31**(0.44) | **92.72**(0.79) | **88.12**(1.24) | **90.18**(0.92) | **75.79**(0.57) | **91.09**(0.76) |

* Significantly different from our MAC-GCN results ($\mathbf{p} < .05$, t-test).

**Table 3**
Performance comparison of different methods using AAL-116 atlas for time series extraction (LMCI vs AD and EMCI vs LMCI).

| Data | Method | LMCI versus AD | | | | | | EMCI versus LMCI | | | | | |
|---|---|---|---|---|---|---|---|---|---|---|---|---|---|
| | | ACC(std.) | SEN(std.) | SPE(std.) | F1(std.) | MCC(std.) | AUC(std.) | ACC(std.) | SEN(std.) | SPE(std.) | F1(std.) | MCC(std.) | AUC(std.) |
| fMRI | RF | 52.12(0.90)* | 46.12(0.86)* | 57.55(0.90)* | 47.24(1.16)* | 20.27(0.72)* | 57.64(1.36)* | 50.62(0.47)* | 50.44(0.49)* | 50.97(0.78)* | 50.50(0.95)* | 20.36(0.59)* | 50.60(0.88)* |
| | SVM | 55.84(1.08)* | 45.88(0.85)* | 60.77(0.78)* | 52.68(0.91)* | 23.64(0.85)* | 63.71(1.64)* | 51.73(0.86)* | 50.18(0.59)* | 53.43(0.53)* | 51.39(0.88)* | 21.48(1.13)* | 57.30(0.77)* |
| | CNN | 56.30(0.72)* | 50.02(0.44)* | 62.11(0.71)* | 61.79(0.66)* | 27.62(1.11)* | 64.87(0.68)* | 56.49(0.75)* | 57.22(0.72)* | 55.98(0.57)* | 54.40(0.74)* | 26.09(0.49)* | 56.40(0.66)* |
| | Transformer | 64.69(0.95)* | 59.65(0.73)* | 71.19(0.81)* | 63.95(0.39)* | 33.76(1.06)* | 64.91(0.78)* | 62.55(0.82)* | 63.16(1.25)* | 61.82(0.69)* | 61.54(0.89)* | 30.06(0.73)* | 62.35(0.69)* |
| | GCN | 62.90(0.93)* | 58.37(0.78)* | 67.23(0.89)* | 60.39(0.69)* | 31.29(0.93)* | 62.60(0.77)* | 62.32(0.60)* | 61.81(0.76)* | 62.97(0.64)* | 60.16(0.58)* | 29.74(0.85)* | 62.19(1.04)* |
| | EX-GCN | 71.19(0.71)* | 69.86(0.67)* | 72.82(0.71)* | 70.38(0.82)* | 36.00(0.80)* | 71.22(0.72)* | 70.34(0.68)* | 58.59(0.81)* | 77.53(1.01)* | 64.14(0.80)* | 32.84(1.92)* | 69.44(0.77)* |
| | MA-GCN | 81.76(0.58)* | 79.72(0.73)* | 84.38(0.63)* | 81.22(0.68)* | 55.95(0.60)* | 81.92(0.85)* | 79.29(0.64)* | 77.42(0.70)* | 80.54(0.61)* | 80.16(0.88)* | 49.04(1.20)* | 79.36(0.55)* |
| | BNT | **86.75**(2.95) | **80.53**(6.06) | **92.00**(5.58) | **84.73**(3.53) | **73.71**(5.78) | **86.26**(2.96) | 71.95(2.17) | 82.10(7.06) | 62.05(8.96) | 74.24(2.00) | 45.49(3.79) | 72.08(2.12) |
| | Com-BNTF | 83.86(2.64) | 80.00(2.35) | 87.11(5.53) | 81.99(2.32) | 67.59(5.17) | 83.56(2.41) | 79.74(2.85) | 76.84(8.81) | **82.56**(5.25) | 78.73(4.06) | **59.92**(5.41) | 79.70(2.90) |
| | BolT | 77.83(11.3) | 80.53(6.34) | 75.56(23.8) | 77.90(8.31) | 57.83(20.6) | 85.24(7.19) | 69.09(6.19) | 76.32(16.5) | 62.05(22.7) | 70.56(5.50) | 40.84(10.0) | 77.81(5.79) |
| | MCA-GCN | 84.76(0.60) | 80.07(0.42) | 89.02(1.33) | 83.04(0.32) | 58.32(0.96) | 84.43(0.61) | **83.01**(0.82) | **84.07**(0.62) | 82.19(0.76) | **83.00**(1.03) | 56.97(0.80) | **83.01**(0.50) |
| Gene | RF | 58.12(0.69)* | 54.60(1.33)* | 61.17(0.60)* | 56.46(1.18)* | 24.23(0.66)* | 66.07(0.73)* | 56.75(0.50)* | 52.75(0.78)* | 60.89(0.89)* | 55.66(0.90)* | 24.77(1.10)* | 65.14(0.44)* |
| | SVM | 60.95(0.70)* | 60.74(1.78)* | 67.08(0.77)* | 60.66(0.57)* | 31.13(0.69)* | 68.13(0.64)* | 60.59(0.61)* | 55.52(0.33)* | 65.86(0.92)* | 61.22(1.26)* | 27.60(1.43)* | 68.39(0.72)* |
| | CNN | 65.73(0.71)* | 65.77(1.02)* | 65.76(0.89)* | 64.66(0.55)* | 35.78(0.56)* | 65.56(0.63)* | 60.96(0.42)* | 56.17(0.43)* | 64.91(1.27)* | 61.20(0.48)* | 32.35(1.17)* | 60.84(0.49)* |
| | Transformer | 67.20(0.93)* | 65.38(0.65)* | 68.79(0.66)* | 67.73(0.82)* | 36.42(0.87)* | 66.04(0.82)* | 61.46(0.72)* | 58.31(1.15)* | 62.97(0.73)* | 60.29(1.37)* | 32.75(0.90)* | 61.30(1.11)* |
| | GCN | 69.52(1.29)* | 68.98(0.78)* | 70.29(0.80)* | 68.53(0.35)* | 37.50(1.33)* | 69.43(0.86)* | 64.06(0.93)* | 62.63(0.52)* | 65.64(1.33)* | 63.89(0.38)* | 32.93(1.14)* | 63.94(0.39)* |
| | EX-GCN | 78.56(0.53)* | 76.03(0.75)* | 80.77(0.72)* | 76.71(0.30)* | 53.82(0.93)* | 78.21(1.07)* | 75.49(0.79)* | 73.91(0.81)* | 77.26(1.45)* | 74.65(0.80)* | 47.16(0.94)* | 75.39(0.41)* |
| | MA-GCN | 81.66(1.21)* | 76.87(0.68)* | 85.39(0.67)* | 77.69(0.74)* | 50.15(0.95)* | 80.93(0.86)* | 79.86(0.48)* | 78.28(0.98)* | 81.35(0.93)* | 79.59(0.90)* | 51.50(0.81)* | 79.72(0.24)* |
| | MCA-GCN | **83.83**(1.40) | **81.05**(0.82) | **86.31**(0.84) | **82.06**(0.57) | **58.58**(1.14) | **83.48**(0.43) | **83.55**(0.85) | **84.60**(0.84) | **82.67**(0.90) | **83.53**(0.67) | **57.32**(0.93) | **83.43**(0.56) |
| Dual | RF | 62.55(2.12)* | 60.44(0.67)* | 64.45(1.36)* | 61.50(0.71)* | 33.53(0.99)* | 66.47(0.33)* | 61.93(0.53)* | 59.86(0.79)* | 64.15(0.79)* | 61.43(0.74)* | 34.31(0.69)* | 66.23(0.55)* |
| | SVM | 67.22(0.52)* | 69.37(0.90)* | 65.40(0.94)* | 66.42(1.36)* | 35.19(0.77)* | 70.20(0.92)* | 66.25(0.76)* | 60.63(1.01)* | 71.07(0.88)* | 66.72(0.77)* | 35.47(0.72)* | 72.07(0.59)* |
| | CNN | 71.43(1.68)* | 69.78(1.45)* | 73.48(0.72)* | 70.76(0.69)* | 41.25(0.87)* | 71.43(0.64)* | 70.52(0.66)* | 67.26(0.70)* | 73.97(1.03)* | 70.71(0.66)* | 40.66(1.34)* | 70.41(0.24)* |
| | Transformer | 72.21(1.29)* | 67.54(0.89)* | 75.18(1.05)* | 71.3(0.67)* | 41.92(0.80)* | 71.75(1.47)* | 71.76(0.85)* | 66.82(0.60)* | 74.49(1.06)* | 71.35(0.99)* | 42.49(1.26)* | 70.98(0.67)* |
| | GCN | 74.42(0.50)* | 71.11(0.74)* | 80.92(0.66)* | 72.55(0.82)* | 45.10(1.02)* | 73.82(0.54)* | 72.09(0.62)* | 71.44(0.79)* | 73.55(1.07)* | 72.02(0.88)* | 44.20(1.12)* | 71.96(0.44)* |
| | EX-GCN | 83.35(1.44)* | 80.68(0.73)* | 83.66(0.93)* | 79.53(0.92)* | 64.87(0.89)* | 82.56(0.74)* | 83.46(0.40)* | 82.55(0.66)* | 84.54(0.89)* | 83.35(0.54)* | 63.56(0.86)* | 83.43(0.46)* |
| | MA-GCN | 88.64(1.55) | 84.76(0.75)* | 91.05(0.68) | 87.25(0.66)* | 68.16(0.86)* | 88.36(0.48)* | 86.95(0.49)* | 86.28(0.55)* | 86.70(1.20)* | 86.87(0.89)* | 64.52(0.98)* | 86.95(0.62)* |
| | MCA-GCN | **90.01**(0.95) | **88.53**(0.72) | **91.20**(0.52) | **89.00**(0.92) | **69.41**(0.92) | **89.29**(0.23) | **88.61**(0.71) | **87.96**(1.02) | **89.21**(1.12) | **88.17**(0.90) | **67.99**(1.10) | **88.59**(0.85) |

* Significantly different from our MAC-GCN results ($\mathbf{p} < .05$, t-test).

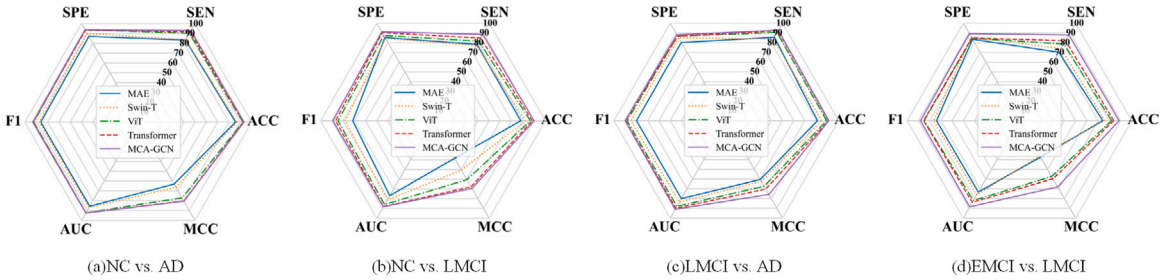


**Fig. 6.** Comparison of Position Encoding Methods in Four Tasks.

### 4.8. Independent center data testing

To further validate the robustness and generalization of the model, we used the ADNI-2 data as an independent test set and the data from the remaining centers (ADNI-GO, ADNI-3, and ADNI-DOD, which include 134 AD, 65 EMCI, and 78 EMCI samples) to train and validate the models. The ratio of training set, validation set and test is set to 6:2:2. We compared our model with the baselines in two classification tasks (LMCI vs AD and EMCI vs LMCI) on the independent test set. The results are shown in Table 9. We observed that although all the methods decrease their performance on the independent test set, MCA-GCN still controls the best ACC, F1, MCC and AUC values in the two classification

**Table 4**
Performance comparison of different methods using Schaefer-400 atlas for time series extraction (NC vs AD and NC vs LMCI).

| Data | Method | NC versus AD | | | | | | NC versus LMCI | | | | | |
|---|---|---|---|---|---|---|---|---|---|---|---|---|---|
| | | ACC(std.) | SEN(std.) | SPE(std.) | F1(std.) | MCC(std.) | AUC(std.) | ACC(std.) | SEN(std.) | SPE(std.) | F1(std.) | MCC(std.) | AUC(std.) |
| fMRI | RF | 52.41(7.16)* | 55.89(8.18)* | 48.85(7.22)* | 54.46(7.02)* | 4.76(14.4)* | 55.62(11.1)* | 52.35(3.76)* | 29.15(6.90)* | 73.26(3.37)* | 36.48(7.27)* | 2.53(8.74) | 53.18(2.76)* |
| | SVM | 54.71(4.85)* | 59.98(9.33)* | 49.31(8.65)* | 57.26(5.59)* | 9.45(10.0)* | 55.88(4.32)* | 54.57(1.83)* | 18.72(3.65)* | 86.87(1.12) | 28.01(5.04)* | 7.49(6.12)* | 55.75(3.62)* |
| | CNN | 58.62(7.49)* | 55.93(34.3) | 61.44(30.5) | 52.79(22.6)* | 20.10(16.8)* | 58.68(7.15)* | 60.99(6.85)* | 44.57(33.9) | 75.43(28.9) | 45.09(28.0)* | 22.61(15.5) | 60.00(7.55)* |
| | Transformer | 57.01(3.41)* | 58.18(30.2) | 55.81(31.7) | 54.67(13.5)* | 09.51(6.94)* | 56.99(3.47)* | 56.05(3.10)* | 56.84(8.85) | 55.34(11.4)* | 54.58(3.87)* | 09.74(3.23)* | 56.10(2.76)* |
| | GCN | 56.09(3.39)* | 33.64(17.1)* | 79.07(13.7) | 41.27(16.2)* | 04.77(3.50)* | 56.35(3.29)* | 54.32(2.89)* | 23.16(13.6)* | 81.86(10.8)* | 40.60(7.84)* | 04.08(2.88)* | 52.51(3.15)* |
| | EX-GCN | 57.93(2.52)* | 61.36(14.6)* | 54.42(14.2)* | 58.99(6.01)* | 09.87(5.92)* | 57.89(2.50)* | 58.27(2.68)* | 22.11(14.7)* | 90.23(11.1) | 31.03(14.4)* | 06.90(3.47)* | 56.17(3.07)* |
| | MA-GCN | 72.64(5.71) | 77.73(17.5) | 67.44(15.0) | 73.44(8.81) | 37.11(13.2) | 72.58(5.67) | 74.07(2.31) | 70.53(3.43)* | 77.21(6.67)* | 71.88(1.44) | 36.29(2.61) | 73.87(2.06) |
| | BNT | 76.78(1.26) | 78.64(6.14) | 74.88(5.55) | 77.34(1.98) | 53.86(2.62) | 76.76(1.24) | 76.05(3.22) | 62.11(6.86) | 88.37(4.03) | 70.73(4.76) | 52.85(6.26) | 75.24(3.35) |
| | Com-BNTF | **81.15**(1.92) | **83.64**(1.90) | **78.60**(4.47) | **81.80**(1.51) | **62.41**(3.74) | **89.40**(1.04) | **79.26**(2.68) | **72.63**(3.00) | 85.12(3.53) | **76.67**(2.90) | **58.44**(5.48) | **82.77**(0.82) |
| | BolT | 77.93(0.96) | 81.36(2.96) | 74.42(3.29) | 78.84(1.05) | 56.02(1.86) | 77.89(0.97) | 73.08(5.05) | 71.05(12.8) | 74.89(16.1) | 71.03(5.05) | 47.29(8.57) | 72.97(4.67) |
| | MCA-GCN | 77.47(5.43) | 79.09(4.37) | 75.81(11.2) | 78.06(4.50) | 43.23(9.19) | 77.45(5.48) | 76.54(1.75) | 57.37(8.20) | **93.49**(5.55) | 69.41(4.08) | 35.07(4.90) | 75.43(2.00) |
| Gene | RF | 61.69(1.55)* | 62.93(0.69)* | 61.31(1.83)* | 61.96(1.77)* | 29.01(0.64)* | 68.64(0.89)* | 59.86(0.88)* | 60.82(0.80)* | 59.34(2.44)* | 58.67(1.28)* | 28.74(0.94)* | 67.11(0.47)* |
| | SVM | 65.89(0.45)* | 59.71(0.78)* | 71.11(1.06)* | 65.51(1.16)* | 34.64(0.41)* | 68.54(0.58)* | 63.06(1.09)* | 69.64(1.19)* | 53.98(0.78)* | 61.23(0.82)* | 31.39(1.68)* | 66.49(0.43)* |
| | CNN | 68.61(0.37)* | 67.90(0.84)* | 69.15(1.72)* | 68.86(0.97)* | 39.99(0.41)* | 68.83(0.48)* | 67.56(0.91)* | 70.45(0.38)* | 64.81(0.88)* | 66.51(1.51)* | 35.96(2.24)* | 67.44(0.75)* |
| | Transformer | 70.38(0.71)* | 69.33(0.71)* | 70.8(1.23)* | 71.34(0.38)* | 41.31(1.30)* | 70.61(1.17)* | 68.64(1.35)* | 73.69(1.26)* | 64.37(0.80)* | 70.22(0.67)* | 35.64(1.38)* | 69.34(0.82)* |
| | GCN | 73.77(0.74)* | 73.07(1.20)* | 75.28(1.61)* | 74.15(0.71)* | 45.44(0.87)* | 73.98(0.52)* | 70.83(0.82)* | 74.06(0.88)* | 70.69(1.00)* | 69.70(2.29)* | 41.25(1.25)* | 70.68(0.80)* |
| | EX-GCN | 82.57(0.29)* | 80.03(0.64)* | 85.22(1.32)* | 83.36(0.74)* | 58.73(0.42)* | 82.50(0.70)* | 80.17(0.81)* | 81.35(0.94)* | 79.33(0.79)* | 79.69(0.63)* | 57.49(1.32)* | 80.22(1.06)* |
| | MA-GCN | 86.48(0.48)* | 83.94(1.05)* | 88.14(1.07) | 87.14(0.80)* | 64.26(0.58)* | 86.42(0.55)* | 84.93(0.75)* | 85.30(0.95)* | 84.72(0.67)* | 84.39(1.22)* | 61.36(1.44)* | 84.89(1.03)* |
| | MCA-GCN | **87.34**(0.60) | **85.84**(0.99) | **89.05**(1.34) | **87.86**(1.08) | **67.14**(0.70) | **87.32**(0.43) | **86.90**(0.69) | **92.34**(0.50) | **85.13**(1.37) | **85.44**(1.05) | **62.08**(0.93) | **86.61**(1.24) |
| | RF | 59.31(3.69)* | 47.68(11.7)* | 71.33(7.06)* | 53.75(9.41)* | 19.58(6.98)* | 59.50(3.67)* | 61.48(1.15)* | 43.79(4.64)* | 77.45(5.05)* | 51.62(1.22)* | 22.90(2.56)* | 67.29(2.31)* |
| | SVM | 57.47(9.16)* | 99.56(0.99) | 13.78(18.6)* | 70.72(4.73)* | 19.50(22.3)* | 67.57(3.11)* | 55.80(2.82)* | 15.12(1.68)* | 92.54(10.6) | 21.32(17.6)* | 13.99(5.66)* | 72.65(3.75)* |
| | CNN | 63.22(14.3)* | 75.39(37.6) | 50.70(47.2)* | 63.45(23.2)* | 31.52(28.0)* | 63.05(14.6)* | 57.04(6.84)* | 42.39(42.5) | 69.78(38.0) | 37.14(34.1)* | 14.72(16.8)* | 56.08(7.52)* |
| | Transformer | 78.39(1.26)* | 90.00(3.45)* | 66.51(4.22)* | 80.81(1.09)* | 52.36(3.86) | 78.25(1.27)* | 61.23(3.56)* | 43.68(10.9)* | 76.74(4.93)* | 50.84(8.00)* | 13.01(5.87)* | 60.21(3.92)* |
| | GCN | 81.15(1.31)* | 80.91(4.13)* | 81.40(5.20)* | 81.27(1.25)* | 50.20(3.16)* | 81.15(1.33)* | 68.40(2.56)* | 67.37(6.06) | 69.30(9.07)* | 66.64(1.77)* | 27.34(2.72)* | 68.34(2.22)* |
| | EX-GCN | 80.23(2.75)* | 70.45(7.87)* | 90.23(5.04)* | 78.10(4.28)* | 43.47(7.14)* | 80.34(2.70)* | 63.95(3.54)* | 48.95(14.1)* | 77.20(10.7) | 55.05(9.99)* | 16.96(5.59)* | 63.08(3.82)* |
| | MA-GCN | 85.05(1.63)* | 84.55(5.42)* | 85.58(5.55)* | 85.09(1.79)* | 59.30(5.54)* | 85.06(1.63)* | 78.77(2.03) | 71.58(7.54) | 85.12(8.48) | 75.91(2.21) | 43.88(4.32) | 78.35(1.85) |
| | MCA-GCN | **94.48**(0.51) | **94.09**(2.03) | **94.88**(1.95) | **94.52**(0.53) | **83.64**(2.32) | **94.49** (0.51) | **80.49**(1.61) | **74.21**(6.81) | **86.05**(8.22) | **78.08**(1.35) | **47.75**(2.82) | **80.13**(1.31) |

* Significantly different from our MAC-GCN results ($\mathbf{p} < .05$, t-test).

**Table 5**
Performance comparison of different methods using Schaefer-400 atlas for time series extraction (LMCI vs AD and EMCI vs LMCI).

| Data | Method | LMCI versus AD | | | | | | EMCI versus LMCI | | | | | |
|---|---|---|---|---|---|---|---|---|---|---|---|---|---|
| | | ACC(std.) | SEN(std.) | SPE(std.) | F1(std.) | MCC(std.) | AUC(std.) | ACC(std.) | SEN(std.) | SPE(std.) | F1(std.) | MCC(std.) | AUC(std.) |
| fMRI | RF | 51.20(3.81)* | 21.36(5.08)* | 77.00(3.16) | 28.79(6.34)* | −2.07(8.94)* | 46.36(2.36)* | 53.41(6.08) | 47.37(8.11) | 59.39(4.86) | 50.16(7.56) | 06.78(12.3) | 51.92(8.10) |
| | SVM | 52.64(3.82)* | 5.16(4.04)* | 93.65(6.31)* | 9.00(6.88)* | −1.36(15.3)* | 47.34(5.92)* | 48.16(3.98)* | 44.74(7.21) | 51.61(5.81)* | 46.03(5.30)* | −3.67(8.01)* | 49.78(2.47)* |
| | CNN | 53.62(0.60)* | 0.0(0.0)* | **100.0**(0.0) | 0.0(0.0)* | 0.0(0.0)* | 50.00(0.0)* | 50.26(0.74)* | 29.47(44.4) | 71.05(44.2) | 23.08(32.2)* | 02.11(1.18)* | 50.26(0.59)* |
| | Transformer | 56.87(4.12)* | 36.32(16.3)* | 74.22(12.6) | 41.91(12.8)* | 08.51(5.08)* | 55.27(4.48)* | 55.06(4.91) | 57.89(16.4) | 52.31(17.6) | 55.07(8.40) | 06.96(7.85) | 55.10(4.88) |
| | GCN | 55.18(1.01)* | 05.26(4.56)* | 97.33(4.82) | 09.22(6.83)* | 02.43(0.84)* | 51.30(0.87)* | 49.14(4.04)* | 22.63(21.0)* | **72.56**(22.1) | 25.49(17.7)* | 0.84(1.77)* | 47.59(3.63)* |
| | EX-GCN | 60.48(1.98) | 27.37(9.23)* | 88.44(7.60) | 38.07(7.94)* | 09.64(2.63)* | 57.90(2.14)* | 58.70(3.60) | 57.37(15.9) | 60.00(19.6) | 57.03(6.14) | **10.82**(4.14) | 58.68(3.48) |
| | MA-GCN | 60.96(2.90) | 48.95(9.95)* | 71.11(9.03) | 53.06(5.79)* | 14.29(3.88)* | 60.03(2.93) | 56.10(5.06) | 54.21(11.3) | 57.94(11.0) | 54.58(6.52) | 07.81(6.46) | 56.08(5.07) |
| | BNT | 61.93(1.08) | 45.79(12.4)* | 75.56(10.4) | 51.67(6.71)* | **22.98**(2.58) | 60.67(1.47) | 49.35(5.59)* | 42.11(11.2) | 56.41(14.5) | 44.51(8.37)* | −1.57(11.3)* | 49.25(5.53)* |
| | Com-BNTF | 59.28(3.45)* | 51.58(14.4) | 65.78(11.1)* | 52.95(8.00)* | 17.91(7.87) | 58.68(3.81)* | 52.21(3.10)* | **65.79**(11.5) | 38.97(11.5)* | **57.31**(4.70) | 05.17(6.58) | 52.38(3.10)* |
| | BolT | 58.79(5.08) | 56.32(5.77) | 60.89(5.58) | 55.59(5.75) | 20.10(8.21) | 62.84(1.19) | 49.35(3.18)* | 52.63(6.15) | 46.15(2.53)* | 50.59(5.02) | −1.25(6.47)* | 50.07(1.53)* |
| | MCA-GCN | **63.37**(3.14) | **61.58**(6.34) | 64.89(7.43) | **60.55**(3.32) | 20.10(4.31) | **63.23**(2.99) | **58.96**(3.96) | 51.05(8.24) | 66.67(8.51) | 54.87(5.89) | 10.09(5.02) | **58.86**(3.96) |
| Gene | RF | 58.12(0.69)* | 54.60(1.33)* | 61.17(0.60)* | 56.46(1.18)* | 24.23(0.66)* | 66.07(0.73)* | 56.75(0.50)* | 52.75(0.78)* | 60.89(0.89)* | 55.66(0.90)* | 24.77(1.10)* | 65.14(0.44)* |
| | SVM | 60.95(0.70)* | 60.74(1.78)* | 67.08(0.77)* | 60.66(0.57)* | 31.13(0.69)* | 68.13(0.64)* | 60.59(0.61)* | 55.52(0.33)* | 65.86(0.92)* | 61.22(1.26)* | 27.60(1.43)* | 68.39(0.72)* |
| | CNN | 65.73(0.71)* | 65.77(1.02)* | 65.76(0.89)* | 64.66(0.55)* | 35.78(0.56)* | 65.56(0.63)* | 60.96(0.42)* | 56.17(0.43)* | 64.91(1.27)* | 61.20(0.48)* | 32.35(1.17)* | 60.84(0.49)* |
| | Transformer | 67.20(0.93)* | 65.38(0.65)* | 68.79(0.66)* | 67.73(0.82)* | 36.42(0.87)* | 66.04(0.82)* | 61.46(0.72)* | 58.31(1.15)* | 62.97(0.73)* | 60.29(1.37)* | 32.75(0.90)* | 61.30(1.11)* |
| | GCN | 69.52(1.29)* | 68.98(0.78)* | 70.29(0.80)* | 68.53(0.35)* | 37.50(1.33)* | 69.43(0.86)* | 64.06(0.93)* | 62.63(0.52)* | 65.64(1.33)* | 63.89(0.38)* | 32.93(1.14)* | 63.94(0.39)* |
| | EX-GCN | 78.56(0.53)* | 76.03(0.75)* | 80.77(0.72)* | 76.71(0.30)* | 53.82(0.93)* | 78.21(1.07)* | 75.49(0.79)* | 73.91(0.81)* | 77.26(1.45)* | 74.65(0.80)* | 47.16(0.94)* | 75.39(0.41)* |
| | MA-GCN | 81.66(1.21)* | 76.87(0.68)* | 85.39(0.67)* | 77.69(0.74)* | 50.15(0.95)* | 80.93(0.86)* | 79.86(0.48)* | 78.28(0.98)* | 81.35(0.93)* | 79.59(0.90)* | 51.50(0.81)* | 79.72(0.24)* |
| | MCA-GCN | **83.83**(1.40) | **81.05**(0.82) | **86.31**(0.84) | **82.06**(0.57) | **58.58**(1.14) | **83.48**(0.43) | **83.55**(0.85) | **84.60**(0.84) | **82.67**(0.90) | **83.53**(0.67) | **57.32**(0.93) | **83.43**(0.56) |
| | RF | 62.79(3.69)* | 41.67(1.84)* | 81.10(3.31) | 50.74(3.75)* | 25.38(7.34)* | 69.00(3.39)* | 56.79(7.56)* | 50.00(4.37)* | 63.47(1.94)* | 53.34(3.45)* | 13.64(17.1)* | 58.01(8.98)* |
| | SVM | 58.21(5.61)* | 13.10(10.9)* | **97.29**(1.91) | 21.41(15.4)* | 18.16(14.4)* | **86.64**(1.18) | 53.89(7.31)* | 16.84(23.7)* | **90.73**(9.67) | 20.64(28.6)* | 4.37(19.8)* | **75.30**(4.20)* |
| | CNN | 57.96(8.73)* | 19.03(36.9)* | 91.39(15.8) | 18.56(32.5)* | 11.18(21.3)* | 55.21(10.6)* | 61.03(8.12)* | 69.47(23.2) | 52.82(21.7)* | 62.40(12.9) | 24.04(15.5) | 61.15(8.02)* |
| | Transformer | 65.06(1.21)* | 52.11(11.8)* | 76.00(10.4) | 57.16(5.56)* | 19.41(3.46)* | 64.05(1.40)* | 63.63(5.36)* | 66.31(25.1) | 61.03(14.9) | 62.10(14.2) | 21.93(14.0) | 63.67(5.59)* |
| | GCN | 69.88(3.40)* | 72.10(4.41)* | 68.00(4.87)* | 68.67(3.44)* | 32.13(5.86)* | 70.05(3.37)* | 64.42(4.74)* | 74.74(12.7) | 54.36(7.99)* | 67.07(6.97) | 23.89(9.30) | 64.55(4.80)* |
| | EX-GCN | 67.71(5.48)* | 58.95(16.3)* | 75.11(8.94) | 61.62(10.9)* | 25.41(10.5)* | 67.03(6.07)* | 65.45(3.85)* | 76.31(15.2) | 54.87(11.6)* | 68.05(6.27) | 26.59(17.7) | 65.59(3.93)* |
| | MA-GCN | 75.42(2.19)* | 77.37(3.00) | 73.78(4.82)* | 74.26(1.86)* | 42.23(3.49)* | 75.57(2.03)* | 68.83(1.84) | **78.95**(18.4) | 58.97(15.6) | 70.73(5.86) | 33.88(13.1) | 68.96(1.98) |
| | MCA-GCN | **81.45**(2.78) | **80.53**(8.03) | 82.22(5.21) | **79.78**(1.30) | **53.39**(8.11) | 81.37(3.00) | **72.98**(6.26) | 71.05(18.1) | 74.87(10.3) | **71.24**(9.85) | **35.42**(16.5) | 72.96(6.37) |

* Significantly different from our MAC-GCN results ($\mathbf{p} < .05$, t-test).

**Table 6**
Ablation study (NC vs AD and NC vs LMCI).

| Data | Method | NC versus AD | | | | | | NC versus LMCI | | | | | |
|---|---|---|---|---|---|---|---|---|---|---|---|---|---|
| | | ACC(std.) | SEN(std.) | SPE(std.) | F1(std.) | MCC(std.) | AUC(std.) | ACC(std.) | SEN(std.) | SPE(std.) | F1(std.) | MCC(std.) | AUC(std.) |
| fMRI | MCA-GCN(no LIA) | 75.24(1.17)* | 74.59(0.59)* | 75.77(0.68)* | 75.31(0.78)* | 39.26(0.52)* | 75.68(0.47)* | 71.23(0.46)* | 75.59(0.87)* | 66.84(0.85)* | 71.40(0.67)* | 32.79(0.84)* | 71.06(0.61)* |
| | MCA-GCN(no MLIF) | 81.58(1.25)* | 82.19(0.55)* | 81.26(0.81)* | 81.55(0.91)* | 57.41(0.46)* | 81.80(0.59)* | 78.34(0.74)* | 82.11(0.39)* | 74.52(1.06)* | 78.29(0.51)* | 45.14(0.91)* | 79.31(0.65)* |
| | MCA-GCN(no Location) | 83.67(0.55)* | 83.19(0.86)* | 85.24(1.14)* | 84.20(0.92)* | 61.62(0.47)* | 84.33(1.02)* | 82.39(0.68)* | 85.24(0.42)* | 79.94(1.33)* | 78.97(0.55)* | 50.31(0.73)* | 80.77(0.58)* |
| | MCA-GCN | **86.22**(0.53) | **84.37**(0.95) | **88.20**(0.81) | **86.39**(1.08) | **65.39**(0.56) | **86.17**(0.54) | **85.67**(0.45) | **87.08**(0.70) | **83.15**(0.95) | **84.25**(0.76) | **61.47**(0.76) | **85.50**(0.85) |
| Gene | MCA-GCN(no LIA) | 82.47(0.82)* | 84.23(0.71)* | 81.75(1.29)* | 83.03(0.83)* | 58.12(0.49)* | 82.45(0.68)* | 79.51(0.54)* | 81.62(0.40)* | 75.92(1.03)* | 78.65(0.34)* | 48.51(0.77)* | 78.03(0.58)* |
| | MCA-GCN(no MLIF) | 84.86(0.87)* | 84.19(0.63)* | 86.24(1.23)* | 85.52(0.78)* | 60.39(0.68)* | 85.08(0.51)* | 84.41(0.36)* | 87.22(0.36)* | 82.67(0.84)* | 83.99(0.50)* | 58.44(0.85)* | 84.43(0.50)* |
| | MCA-GCN | **87.34**(0.60) | **85.84**(0.99) | **89.05**(1.34) | **87.86**(1.08) | **67.14**(0.70) | **87.32**(0.43) | **86.90**(0.69) | **92.34**(0.50) | **85.13**(1.37) | **85.44**(1.05) | **62.08**(0.93) | **86.61**(1.24) |
| Dual | MCA-GCN(no LIA) | 86.72(0.76)* | 85.14(1.47)* | 86.77(1.26)* | 85.59(0.92)* | 64.27(0.81)* | 85.65(0.47)* | 84.38(0.69)* | 88.99(0.77)* | 85.46(0.76)* | 85.56(0.84)* | 61.30(0.78)* | 84.23(0.62)* |
| | MCA-GCN(no MLIF) | 90.54(0.90)* | 89.33(1.02)* | 90.67(0.82)* | 90.75(1.14)* | 76.93(0.86)* | 90.71(0.49)* | 88.76(0.70)* | 90.14(0.78)* | 87.19(0.73) | 88.09(0.93)* | 65.86(0.79)* | 88.66(0.65)* |
| | MCA-GCN(no Location) | 92.36(0.60)* | 91.74(0.98)* | 92.64(0.81)* | 92.31(0.86) | 79.11(0.56)* | 92.17(0.61) | 89.14(0.60)* | 92.26(0.64) | 84.31(0.82)* | 87.59(0.69)* | 73.15(1.00)* | 88.78(0.90)* |
| | MCA-GCN | **93.27**(0.59) | **92.98**(1.04) | **93.89**(1.16) | **93.12**(0.97) | **80.59**(0.91) | **92.55**(0.65) | **91.31**(0.44) | **92.72**(0.79) | **88.12**(1.24) | **90.18**(0.92) | **75.79**(0.57) | **91.09**(0.76) |

* Significantly different from the non-bold values ($\mathbf{p} < .05$, t-test).

**Table 7**
Ablation study (LMCI vs AD and EMCI vs LMCI).

| Data | Method | LMCI versus AD | | | | | | EMCI versus LMCI | | | | | |
|---|---|---|---|---|---|---|---|---|---|---|---|---|---|
| | | ACC(std.) | SEN(std.) | SPE(std.) | F1(std.) | MCC(std.) | AUC(std.) | ACC(std.) | SEN(std.) | SPE(std.) | F1(std.) | MCC(std.) | AUC(std.) |
| fMRI | MCA-GCN (no LIA) | 69.11(0.81)* | 64.07(0.67)* | 74.61(0.43)* | 66.37(0.79)* | 29.64(0.91)* | 69.33(0.77)* | 65.97(0.95)* | 66.58(0.40)* | 65.24(0.95)* | 64.96(1.31)* | 25.42(0.72)* | 65.77(0.30)* |
| | MCA-GCN (no MLIF) | 75.34(0.77)* | 76.89(1.02)* | 75.86(0.75)* | 76.24(0.50)* | 44.86(0.76)* | 76.38(0.60)* | 74.84(0.90)* | 72.06(0.53)* | 79.74(0.91)* | 72.36(0.98)* | 44.19(0.80)* | 74.27(0.59)* |
| | MCA-GCN (no Location) | 80.66(0.66)* | 78.84(0.96)* | 86.69(0.86)* | 78.65(0.90)* | 48.63(0.74)* | 80.33(0.57)* | 78.62(0.83)* | 81.94(0.76)* | 78.85(0.78)* | 80.22(0.96)* | 50.08(0.52)* | 78.64(0.60)* |
| | MCA-GCN | **84.76(0.60)** | **80.07(0.42)** | **89.02(1.33)** | **83.04(0.32)** | **58.32(0.96)** | **84.43(0.61)** | **83.01(0.82)** | **84.07(0.62)** | **82.19(0.76)** | **83.00(1.03)** | **56.97(0.80)** | **83.01(0.50)** |
| Gene | MCA-GCN (no LIA) | 75.08(0.94)* | 74.55(0.80)* | 76.31(0.72)* | 74.62(0.88)* | 46.83(0.76)* | 75.61(0.70)* | 72.69(0.89)* | 68.91(0.83)* | 72.94(0.72)* | 71.33(0.94)* | 45.07(0.72)* | 71.64(0.64)* |
| | MCA-GCN (no MLIF) | 80.64(0.63)* | 80.76(0.82) | 81.89(0.79)* | 80.06(0.81)* | 56.69(1.03)* | 81.05(0.68)* | 78.66(0.76)* | 76.65(0.53)* | 80.61(0.52)* | 78.07(0.82)* | 51.39(0.83)* | 79.24(0.62)* |
| | MCA-GCN | **83.83(1.40)** | **81.05(0.82)** | **86.31(0.84)** | **82.06(0.57)** | **58.58(1.14)** | **83.48(0.43)** | **83.55(0.85)** | **84.60(0.84)** | **82.67(0.90)** | **83.53(0.67)** | **57.32(0.93)** | **83.43(0.56)** |
| Dual | MCA-GCN (no LIA) | 82.22(0.85)* | 81.03(0.82)* | 84.92(0.77)* | 81.89(0.71)* | 60.04(0.87)* | 82.74(0.48)* | 82.03(0.88)* | 79.43(0.60)* | 85.67(0.89)* | 82.55(0.60)* | 61.79(0.97)* | 82.31(0.52)* |
| | MCA-GCN (no MLIF) | 86.73(0.92)* | 83.51(0.76)* | 89.82(0.60)* | 86.17(0.75)* | 67.82(0.81)* | 86.41(0.51)* | 85.27(0.97)* | 82.16(0.96)* | 87.30(0.96)* | 85.42(0.76)* | 65.38(1.15)* | 85.51(0.90)* |
| | MCA-GCN (no Location) | 86.55(0.83)* | 82.72(0.75)* | 89.79(0.64)* | 83.66(0.93)* | 65.58(0.67)* | 85.87(0.40)* | 85.33(0.99)* | 84.43(1.01)* | 86.09(0.83)* | 85.14(0.83)* | 66.24(0.80)* | 86.03(1.03)* |
| | MCA-GCN | **90.01(0.95)** | **88.53(0.72)** | **91.20(0.52)** | **89.00(0.92)** | **69.41(0.92)** | **87.29(0.23)** | **88.61(0.71)** | **87.96(1.02)** | **89.21(1.12)** | **88.17(0.90)** | **67.99(1.10)** | **88.59(0.85)** |

* Significantly different from the non-bold values ($p < .05$, t-test).

**Table 8**
Comparison with other advanced methods.

| Method | Attention | Modality | MRI input format | Subjects | ACC | AUC |
|---|---|---|---|---|---|---|
| Zhou et al. (2020) | No | MRI+PET | Jacob atlas, time series of 93 ROIs | 226 (NC)/362 (MCI) | 0.746 | 0.748 |
| | | | | 362 (MCI)/186 (AD) | 0.748 | 0.755 |
| Xing et al. (2020) | Yes | MRI | 3D MRI data, no time series of ROIs extracted | 51 (NC)/49 (AD) | 0.910 | / |
| Gan et al. (2021) | No | fMRI | AAL atlas, time series of 116 ROIs | 48 (NC)/59 (AD) | 0.888 | 0.902 |
| Bi, Wang, et al. (2022) | No | fMRI+SNP | AAL atlas, time series of 116 ROIs | 237 (NC)/233 (AD) | 0.882 | 0.907 |
| | | | | 197 (EMCI)/203 (LMCI) | 0.838 | 0.862 |
| | | | | 203 (LMCI)/233 (AD) | 0.851 | 0.870 |
| Wang, Li, et al. (2022) | Yes | MRI+SNP | 3D MRI data, no time series of ROIs extracted | 205 (NC)/174 (AD) | 0.838 | 0.924 |
| Bi, Zhou, et al. (2022) | No | fMRI+SNP | AAL atlas, time series of 116 ROIs | 237 (NC)/233 (AD) | 0.894 | 0.914 |
| | | | | 197 (EMCI)/203 (LMCI) | 0.850 | 0.884 |
| | | | | 203 (LMCI)/233 (AD) | 0.864 | 0.902 |
| Tian et al. (2023) | Yes | DTI+fMRI+T1 | AAL atlas, time series of 116 ROIs | 167(NC)/191(AD) | 0.857 | 0.859 |
| | | | | 160(MCI)/191(AD) | 0.801 | 0.793 |
| | | | | 160(MCI)/167(NC) | 0.775 | 0.777 |
| Bi et al. (2023) | No | fMRI+SNP | AAL atlas, time series of 116 ROIs | 237 (NC)/233 (AD) | 0.883 | / |
| | | | | 197 (EMCI)/203 (LMCI) | 0.838 | / |
| | | | | 203 (LMCI)/233 (AD) | 0.849 | / |
| Qin et al. (2022) | Yes | MRI | 3D MRI data, no time series of ROIs extracted | 114 (NC)/98 (AD) | 0.927 | / |
| MCA-GCN | Yes | fMRI+SNP | AAL and Schaefer atlas, time series of 116/ 400 ROIs | 213 (NC)/222 (AD) | 0.932 | 0.926 |
| | | | | 213 (NC)/192 (LMCI) | 0.913 | 0.911 |
| | | | | 192 (LMCI)/222 (AD) | 0.900 | 0.893 |
| | | | | 190 (EMCI)/192 (LMCI) | 0.886 | 0.886 |

tasks. This indicates the outperformance of MCA-GCN than the baseline method on the independent test set.

### 4.9. Pathogenic brain regions and genes

We extracted the causative brain regions and genes associated with AD classification by calculating feature scores at multiple stages of the model, which enabled the interpretation of the diagnostic results. Tables 10 and 11 show the important brain regions and genes that distinguish NC and AD patients, and Fig. 7 shows the location of these brain regions in the brain. Figs. 8 and 9 illustrate the highly pathogenic brain regions and genes found in the four prediction tasks. We note that there is a high degree of consistency in the pathogenic brain regions and pathogenic genes identified by MCA-GCN across different predictions.

Brain regions PHG.R (parahippocampal gyrus, right), HIP.R (hippocampus, right), and INS.L (insula, left) contributed significantly in all four categorization tasks. The parahippocampal gyrus is one of the structures in the brain that is closely associated with memory formation

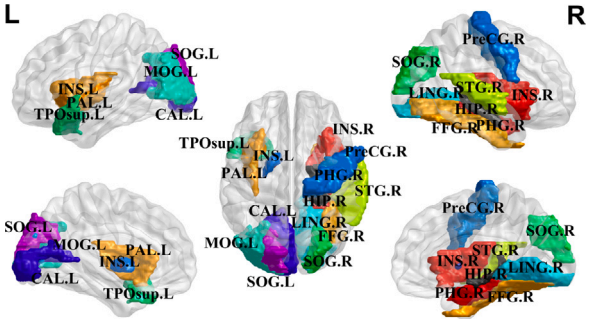


**Fig. 7.** Location of significant pathogenic brain regions.

**Table 9**
Classification performance of different comparison methods on ADNI-2 database.

| Data | Method | LMCI versus AD | | | | | | EMCI versus LMCI | | | | | |
|---|---|---|---|---|---|---|---|---|---|---|---|---|---|
| | | ACC(std.) | SEN(std.) | SPE(std.) | F1(std.) | MCC(std.) | AUC(std.) | ACC(std.) | SEN(std.) | SPE(std.) | F1(std.) | MCC(std.) | AUC(std.) |
| fMRI | RF | 51.06(0.84)* | 27.12(0.93)* | 97.16(0.90) | 47.91(0.36)* | 14.20(0.95)* | 50.60(0.98)* | 50.89(0.42)* | 82.90(1.25)* | 47.58(0.78)* | 53.74(0.95)* | 14.17(0.75)* | 50.95(1.15)* |
| | SVM | 54.78(0.76)* | 26.88(0.64)* | **98.34(0.99)** | 51.15(0.96)* | 17.57(0.98)* | 55.67(1.10)* | 52.34(0.75)* | 82.64(0.69)* | 52.04(1.06)* | 53.63(0.52)* | 13.29(1.40)* | 52.65(1.34)* |
| | CNN | 55.24(1.42)* | 31.02(0.53)* | 97.76(0.60) | 55.99(0.63) | 21.55(0.44)* | 56.83(0.52)* | 54.10(1.09)* | 83.68(0.70) | 48.59(0.98)* | 57.64(0.70)* | 15.90(1.07)* | 55.75(1.23)* |
| | Transformer | 63.53(0.83)* | **40.65(1.16)** | 95.85(1.11)* | 55.87(1.08) | 27.69(0.76) | 62.87(0.76)* | 60.16(0.72)* | **84.62(1.26)** | 54.43(0.60)* | 61.78(0.63)* | 19.87(1.15)* | 60.70(0.45)* |
| | GCN | 61.74(0.67)* | 39.37(0.74) | 97.23(1.06) | 54.59(1.37) | 25.22(0.97)* | 60.56(0.89)* | 59.93(0.90)* | 84.27(0.54) | 55.58(1.36) | 60.40(0.92)* | 19.55(1.28)* | 60.54(0.99)* |
| | EX-GCN | 61.28(1.31)* | 37.33(1.29)* | 97.61(0.83) | 49.74(0.81)* | 23.16(0.56)* | 61.32(0.26)* | 63.96(0.67)* | 81.05(1.14)* | 50.14(0.46)* | 64.38(1.62)* | 22.65(1.35)* | 63.79(0.70)* |
| | MA-GCN | 65.59(0.98)* | 49.62(1.07) | 95.55(0.98)* | 52.67(0.61)* | 27.29(1.26) | 64.54(1.08)* | 64.91(1.39)* | 82.88(0.92)* | 53.15(0.55)* | 66.40(0.85)* | 24.85(0.92)* | 64.71(0.67)* |
| | MCA-GCN | **67.67(0.83)** | 40.00(0.77) | 98.26(1.33) | **58.15(0.76)** | **28.52(1.46)** | **67.26(0.79)** | **66.63(1.00)** | 84.53(0.82) | **55.80(1.42)** | **69.24**(1.16) | **26.97**(1.03) | **67.36**(1.21) |
| Gene | RF | 56.42(0.59)* | 24.03(1.13)* | 98.15(1.21) | 48.74(1.20)* | 18.60(0.83)* | 55.97(0.93)* | 51.57(1.32)* | 80.41(0.63)* | 47.20(1.39)* | 51.89(0.61)* | 14.08(0.74)* | 50.45(0.97)* |
| | SVM | 55.28(0.87)* | 24.91(0.93)* | 97.63(0.91) | 47.22(1.20)* | 16.43(1.52)* | 54.35(0.66)* | 55.41(0.47)* | 83.18(0.93)* | 54.17(0.76)* | 55.45(1.09)* | 17.91(0.97)* | 53.70(1.09)* |
| | CNN | 56.08(0.76)* | 22.27(1.16)* | 96.28(1.01)* | 47.91(1.03)* | 16.62(0.77)* | 56.37(0.47)* | 55.78(0.99)* | 83.83(1.02)* | 53.22(1.16)* | 55.43(0.62)* | 16.66(0.84)* | 56.15(0.74)* |
| | Transformer | 57.30(0.63)* | 23.15(1.08)* | **98.46(0.92)** | 48.37(0.55)* | 17.28(0.74)* | 57.49(0.88)* | 56.28(1.03)* | 84.97(1.11)* | 51.28(0.57)* | 54.52(0.87)* | 18.06(0.83)* | 56.61(0.90)* |
| | GCN | 57.48(1.22)* | 21.16(0.88)* | 97.64(0.98) | 49.31(0.80)* | 17.95(0.90)* | 56.34(1.31)* | 58.88(0.75)* | 83.29(1.30)* | 53.95(1.00)* | 58.12(0.88)* | 17.24(0.48)* | 59.25(0.82)* |
| | EX-GCN | 62.59(0.92)* | 27.18(0.78)* | 98.12(1.23) | 48.29(0.97)* | 21.02(1.03)* | 62.25(0.64)* | 61.02(0.55)* | 81.57(0.72)* | 55.57(0.95) | 59.01(1.13)* | 24.47(0.60)* | 60.70(0.73)* |
| | MA-GCN | 66.67(0.88)* | 34.07(1.06)* | 98.26(0.67) | 53.71(0.99)* | 25.88(0.93)* | 66.66(1.54) | 65.39(0.83)* | 83.94(1.11)* | 54.66(0.96)* | 65.95(0.90)* | 31.81(0.49)* | 65.03(0.87)* |
| | MCA-GCN | **68.15(1.03)** | **38.52(0.30)** | 97.78(1.48) | **55.19(0.71)** | **27.93(0.71)** | **68.48(1.93)** | **69.08(0.51)** | **85.26(1.04)** | **56.67(0.93)** | **68.89(0.91)** | **37.29(0.75)** | **68.74(1.22)** |
| Dual | RF | 56.64(1.01)* | 27.34(1.07)* | 98.45(0.94) | 55.34(0.98)* | 16.37(0.98)* | 56.45(1.08)* | 58.79(0.94)* | 84.53(1.03)* | 54.94(1.00) | 57.95(0.76)* | 17.97(0.98)* | 58.60(0.47)* |
| | SVM | 57.18(1.22)* | 25.14(0.39)* | 96.67(0.92)* | 52.77(1.30)* | 17.19(0.60)* | 58.61(0.95)* | 57.11(0.78)* | 85.30(1.17)* | 52.86(0.33) | 60.24(1.47)* | 19.13(1.04)* | 58.44(0.47)* |
| | CNN | 61.33(0.47)* | 26.48(0.46)* | 97.96(1.19) | 53.14(1.28)* | 21.47(0.93)* | 61.05(0.84)* | 61.38(0.94)* | 82.93(1.28)* | 53.76(1.17) | 64.23(0.76)* | 24.32(0.87)* | 61.78(0.69)* |
| | Transformer | 61.24(1.23)* | 31.36(1.02)* | **98.77(0.86)** | 52.30(0.73)* | 21.49(0.48)* | 61.57(1.62)* | 62.62(0.68)* | 84.49(0.80)* | 54.94(1.29) | 64.87(0.86)* | 26.15(0.86)* | 62.35(1.37)* |
| | GCN | 65.93(1.34)* | 33.33(0.59)* | 97.85(1.00) | 56.83(1.04)* | 26.37(0.84)* | 65.59(0.75)* | 62.95(0.83)* | 86.11(0.98) | 52.31(1.24) | 65.54(0.80)* | 27.86(1.46)* | 61.33(1.32)* |
| | EX-GCN | 68.89(0.50)* | 38.52(0.78)* | 98.26(0.86) | 57.58(1.10)* | 28.94(0.99)* | 68.33(0.65)* | 64.32(0.92)* | 82.76(0.59)* | **56.61(1.22)** | 69.53(1.02)* | 34.22(0.48)* | 64.80(1.12)* |
| | MA-GCN | 71.27(0.74)* | 43.70(0.99)* | 97.18(0.91)* | 61.49(0.72)* | 32.71(0.76)* | 71.27(0.80)* | 67.81(1.15)* | 86.49(0.63) | 55.56(1.02) | 72.05(0.97)* | 37.41(0.60)* | 67.35(1.02)* |
| | MCA-GCN | **73.70(1.18)** | **48.89(0.97)** | 98.52(0.81) | **65.54(1.04)** | **37.45(1.04)** | **73.89(0.85)** | **71.11(1.09)** | **86.67(0.90)** | 53.33(1.08) | **74.31(1.20)** | **39.64(0.88)** | **71.37(1.38)** |

* Significantly different from the non-bold values ($p < .05$, t-test).

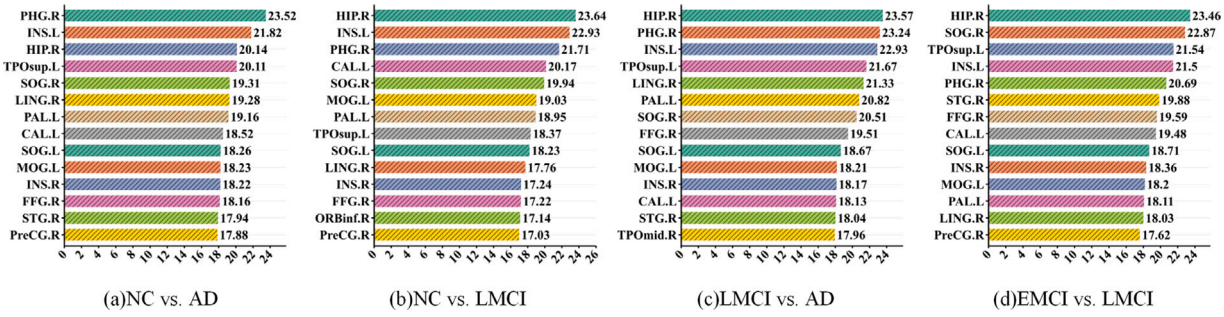


**Fig. 8.** Risk brain regions identified in four categorization tasks.

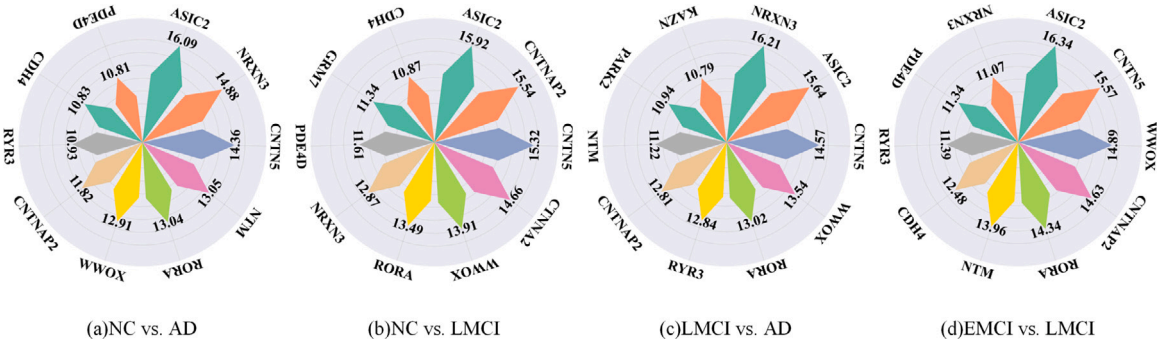


**Fig. 9.** Risk genes identified in four classification tasks.

and storage, and numerous studies have shown that the parahippocampal gyrus is severely impaired in patients with Alzheimer's disease, resulting in impaired memory function (Teipel, Fritz, Grothe, & Initiative, 2020). The hippocampus is one of the first regions to show signs of AD neuropathology, which is involved in the process of AD memory degradation and, in advanced cases, is the most profoundly affected region (West, Coleman, Flood, & Troncoso, 1994; Yi, Jin, Xu, Wei, & Rui, 2021). The insula is a deep brain structure involved in a variety of cognitive and emotional processes. It is closely associated with emotion regulation, social cognition and self-awareness. People with Alzheimer's disease typically experience cognitive and emotional problems such as memory loss, emotional apathy and interpersonal difficulties (Rosenberg, Nowrangi, & Lyketsos, 2015).

ASIC2, CNTN5 have high contribution in all four classification tasks. The ASIC gene family is widely expressed in the mammalian nervous system, especially in the brain (Cherninskyi, Storozhuk, Maximyuk, Kulyk, & Krishtal, 2023). Increasing evidence suggests that ASIC activation may be a factor in AD progression (Gonzales & Sumien, 2017; Mango & Nisticò, 2021). CNTN5 has been implicated in the regulation of certain neuronal orientations and the organization of axon-axon connections (Ashrafi et al., 2014). In previous AD studies, CNTN5 variants were determined to be associated with white matter lesion (WML) volume, entorhinal cortex thickness (ECT), parahippocampal gyrus thickness, and temporal pole cortex thickness (TPT) (Biffi et al., 2010).

To investigate the relationship between the extracted pathogenic brain regions and pathogenic genes, we calculated the Pearson correlation coefficients between pathogenic brain-region time series and pathogenic gene SNP coding in the AD and NC samples, respectively, and then analyzed the significantly different associations between the

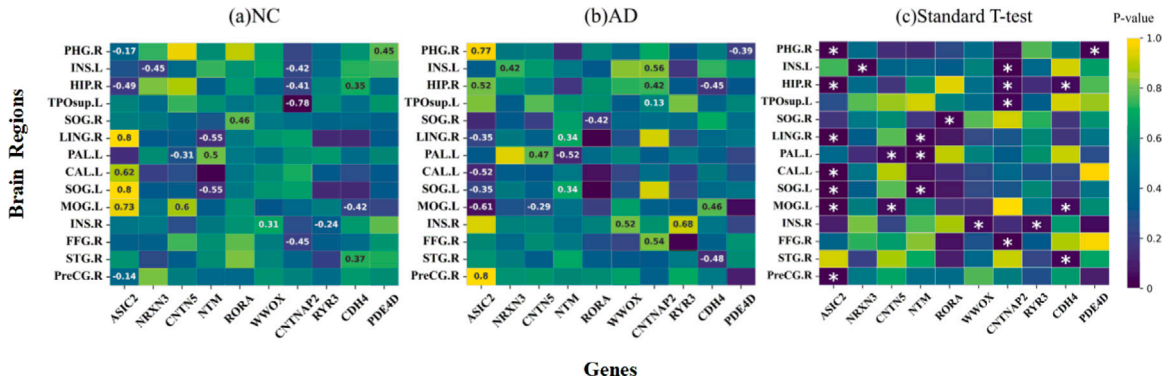


**Fig. 10.** Heatmap showing brain region-gene pairs of P -values in the NC(a),AD(b) group. Marked with an asterisk when $p < 0.05$(c).

**Table 10**
Significantly pathogenic brain regions in NC vs AD.

| Brain area | Full name of the brain region | Pathogenicity score |
|---|---|---|
| PHG.R | Parahippocampal gyrus Right | 23.52 |
| INS.L | Insula Left | 21.82 |
| HIP.R | Hippocampus Right | 20.14 |
| TPOsup.L | Temporal pole: superior temporal gyrus Left | 20.12 |
| SOG.R | Superior occipital gyrus Right | 19.31 |
| LING.R | Lingual gyrus Right | 19.28 |
| PAL.L | Lenticular nucleus pallidum Left | 19.16 |
| CAL.L | Calcarine fissure and surrounding cortex Left | 18.52 |
| SOG.L | Superior occipital gyrus Left | 18.26 |
| MOG.L | Middle occipital gyrus Left | 18.23 |
| INS.R | Insula Right | 18.22 |
| FFG.R | Fusiform gyrus Right | 18.16 |
| STG.R | Superior temporal gyrus Right | 17.94 |
| PreCG.R | Precentral gyrus Right | 17.88 |

**Table 11**
Significantly pathogenic genes for NC vs AD.

| Gene | Full name of gene | Pathogenicity score |
|---|---|---|
| ASIC2 | Acid Sensing Ion Channel Subunit 2 | 16.09 |
| NRXN3 | Neurexin 3 | 14.88 |
| CNTN5 | Contactin 5 | 14.36 |
| NTM | Neurotrimin | 13.05 |
| RORA | RAR Related Orphan Receptor A | 13.04 |
| WWOX | WW Domain Containing Oxidoreductase | 12.91 |
| CNTNAP2 | Contactin Associated Protein 2 | 11.82 |
| RYR3 | Ryanodine Receptor 3 | 10.93 |
| CDH4 | Cadherin 4 | 10.83 |
| PDE4D | Phosphodiesterase 4D | 10.81 |

two groups of samples by standardized T-test. Fig. 10(c) demonstrates the pathogenic brain region-gene associations that are very different in AD and NC samples ($P < 0.05$, marked with an asterisk). We observed differential associations between the brain region PHG.R (right parahippocampal gyrus) and the genes ASCI2 and PDE4D in AD and NC samples. The genes significantly associated with HIP.R (hippocampus, right) were ASCI2, CNTNAP2, and CDH4. Among these genes, the gene ASCI2 was significantly associated with several brain regions, including PHG.R (Parahippocampal gyrus Right), HIP.R (Hippocampus Right), LING.R (Lingual gyrus Right), CAL.R (Calcarine fissure and surrounding cortex Left), SOG.L (Superior occipital gyrus Left), MOG.L (Middle occipital gyrus Left), and PreCG.R (Precentral gyrus Right). Figs. 10(a) and 10(b) show the association between NC and PCC values of significantly different associations between pathogenic brain regions and genes in AD patients, respectively. These results suggest that the association between pathogenic brain regions and genes extracted by MCA-GCN differed between the two types of samples. Our approach finds patterns of brain region and gene associations that distinguish AD patients. Interestingly, we noticed that the gene ASCI2 had a small correlation coefficient with the brain region PreCG.R in NC ($PCC = -0.14$), whereas in AD they had a higher correlation coefficient ($PCC = 0.8$). On the other hand, the correlation coefficient of ASCI2 gene with brain regions LING.R and SOG.L was higher in NC ($PCC = 0.8$) and lower in AD ($PCC = -0.35$). These provide a reference for exploring the pathogenesis of AD and finding therapeutic targets.

To further analyze the significant brain regions and genes identified by the MCA-GCN in the four tasks, the significant factors were compared with existing imaging genetics studies, and as shown in Table 12, most of the significant brain regions and genes were validated in the literature, especially in the NC-AD group.

## 5. Conclusion

This work proposed MCA-GCN incorporating a multi-stream cross-attention and graph convolutional network for Alzheimer's disease diagnosis and pathogenesis gene and brain-region identification. This model can learn brain region-gene associations from long-range and local aspects, providing a more comprehensive view of their relationships.

The model also introduces a learnable position encoding method that combines absolute and relative position information of fMRI time points to generate brain region embeddings containing dynamic information. In addition, the model explains classification and diagnostic results by calculating weights for brain regions and genes based on their importance or relevance to the classification task. Experimental results on the ADNI dataset show that the model outperforms competing methods on four independent classification tasks and can identify some brain regions and genes associated with Alzheimer's disease. The model provides a new perspective and tool for the study of Alzheimer's disease and the analysis of other neurodegenerative diseases.

However, due to the scarcity of data, there remains significant potential for development in the utilization of multimodal data. In our future work, we plan to explore innovative methodologies for effectively measuring non-linear relationships between genes and brain

**Table 12**
Brain regions and genes for which the four categorization tasks remain significant in other imaging genetics articles.

| NC versus AD | | NC versus LMCI | | LMCI versus AD | | EMCI versus LMCI | |
|---|---|---|---|---|---|---|---|
| ROIs | Genes | ROIs | Genes | ROIs | Genes | ROIs | Genes |
| PHG.R (Bi, Hu, et al., 2020; Bi et al., 2023) | ASIC2 (Bi, Hu, et al., 2020; Bi et al., 2023; Bi, Mao, et al., 2022; Bi, Wang, et al., 2022; Bi, Zhou, et al., 2022) | HIP.R (Bi, Liu, Xie, Hu, & Jiang, 2020) | ASIC2 (Bi, Liu, et al., 2020) | INS.L (Bi et al., 2024) | WWOX (Bi et al., 2024) | SOG.R (Bi, Li, et al., 2022) | ASIC2 (Bi, Li, et al., 2022) |
| SOG.R (Bi et al., 2023; Bi, Mao, et al., 2022; Bi, Wang, et al., 2022; Bi, Zhou, et al., 2022) | CNTN5 (Bi, Hu, et al., 2020; Bi et al., 2023; Bi, Wang, et al., 2022; Bi, Zhou, et al., 2022) | MOG.L (Bi, Liu, et al., 2020) | CNTNAP2 (Bi, Liu, et al., 2020) | SOG.R (Bi et al., 2024) | | PreCG.R (Bi, Li, et al., 2022) | NRXN3 (Bi, Li, et al., 2022) |
| LING.R (Bi, Hu, et al., 2020) | NTM (Bi, Hu, et al., 2020) | INS.R (Bi, Liu, et al., 2020) | CNTN5 (Bi, Liu, et al., 2020) | | | | |
| CAL.L (Bi, Hu, et al., 2020) | WWOX (Bi, Hu, et al., 2020) | | WWOX (Bi, Liu, et al., 2020) | | | | |
| MOG.L (Bi, Wang, et al., 2022) | CNTNAP2 (Bi, Hu, et al., 2020; Bi et al., 2023; Bi, Mao, et al., 2022; Bi, Wang, et al., 2022; Bi, Zhou, et al., 2022) | | GRM7 (Bi, Liu, et al., 2020) | | | | |
| INS.R (Bi, Hu, et al., 2020) | | | | | | | |
| PreCG.R (Bi, Mao, et al., 2022; Bi, Wang, et al., 2022; Bi, Zhou, et al., 2022) | | | | | | | |

areas,involves incorporating advanced activation functions or considering dynamic weighting networks, allowing for adaptive adjustments to the significance of various features based on contextual information and the specific characteristics of the input data. This adaptability could provide a more nuanced understanding of the interactions between brain regions and genes.

## CRediT authorship contribution statement

**Wei Peng:** Writing – review & editing, Writing – original draft, Methodology, Funding acquisition, Conceptualization. **Yanhan Ma:** Data curation, Software. **Chunshan Li:** Writing – original draft, Software, Methodology. **Wei Dai:** Writing – review & editing, Supervision, Conceptualization. **Xiaodong Fu:** Validation, Conceptualization. **Li Liu:** Validation, Conceptualization. **Lijun Liu:** Validation, Conceptualization. **Jin Liu:** Resources, Project administration.

## Declaration of competing interest

The authors declare the following financial interests/personal relationships which may be considered as potential competing interests: Wei Peng reports article publishing charges was provided by National Natural Science Foundation of China. If there are other authors, they declare that they have no known competing financial interests or personal relationships that could have appeared to influence the work reported in this paper.

## Acknowledgments

This work was supported in part by the National Natural Science Foundation of China under Grant 62472202, 62172444, 62472450, 61972185, and in part by Yunnan Ten Thousand Talents Plan Young.

## Data availability

The data can be downloaded from ADNI:https://adni.loni.usc.edu/ The sourcecode are available at:https://github.com/weiba/MCAGCN.

## References

Abbas, S. Qasim, Chi, Lianhua, & Chen, Yi-Ping Phoebe (2023). Transformed domain convolutional neural network for Alzheimer's disease diagnosis using structural MRI. *Pattern Recognition*, *133*, Article 109031.

Alexander-Bloch, Aaron, Giedd, Jay N., & Bullmore, Ed (2013). Imaging structural co-variance between human brain regions. *Nature Reviews. Neuroscience*, *14*(5), 322–336.

Arranz, Amaia M., & De Strooper, Bart (2019). The role of astroglia in Alzheimer's disease: pathophysiology and clinical implications. *The Lancet Neurology*, *18*(4), 406–414.

Ashrafi, Soha, Betley, J Nicholas, Comer, John D, Brenner-Morton, Susan, Bar, Vered, Shimoda, Yasushi, et al. (2014). Neuronal Ig/Caspr recognition promotes the formation of axoaxonic synapses in mouse spinal cord. *Neuron*, *81*(1), 120–129.

Bannadabhavi, Anushree, Lee, Soojin, Deng, Wenlong, Ying, Rex, & Li, Xiaoxiao (2023). Community-aware transformer for autism prediction in fmri connectome. In *International conference on medical image computing and computer-assisted intervention* (pp. 287–297). Springer.

Batmanghelich, Nematollah K, Dalca, Adrian, Quon, Gerald, Sabuncu, Mert, & Golland, Polina (2016). Probabilistic modeling of imaging, genetics and diagnosis. *IEEE Transactions on Medical Imaging*, *35*(7), 1765–1779.

Bedel, Hasan A, Sivgin, Irmak, Dalmaz, Onat, Dar, Salman UH, & Çukur, Tolga (2023). Bolt: Fused window transformers for fMRI time series analysis. *Medical Image Analysis*, *88*, Article 102841.

Bellenguez, Céline, Küçükali, Fahri, Jansen, Iris E, Kleineidam, Luca, Moreno-Grau, Sonia, Amin, Najaf, et al. (2022). New insights into the genetic etiology of Alzheimer's disease and related dementias. *Nature Genetics*, *54*(4), 412–436.

Bi, Xia-an, Hu, Xi, Wu, Hao, & Wang, Yang (2020). Multimodal data analysis of Alzheimer's disease based on clustering evolutionary random forest. *IEEE Journal of Biomedical and Health Informatics*, *24*(10), 2973–2983.

Bi, Xia-an, Li, Lou, Wang, Zizheng, Wang, Yu, Luo, Xun, & Xu, Luyun (2022). IHGC-GAN: influence hypergraph convolutional generative adversarial network for risk prediction of late mild cognitive impairment based on imaging genetic data. *Briefings in Bioinformatics*, *23*(3), bbac093.

Bi, Xia-an, Liu, Yingchao, Xie, Yiming, Hu, Xi, & Jiang, Qinghua (2020). Morbigenous brain region and gene detection with a genetically evolved random neural network cluster approach in late mild cognitive impairment. *Bioinformatics*, *36*(8), 2561–2568.

Bi, Xia-an, Luo, Sheng, Jiang, Siyu, Wang, Yu, Xing, Zhaoxu, & Xu, Luyun (2023). Explainable and programmable hypergraph convolutional network for imaging genetics data fusion. *Information Fusion*, *100*, Article 101950.

Bi, Xia-an, Mao, Yuhua, Luo, Sheng, Wu, Hao, Zhang, Lixia, Luo, Xun, et al. (2022). A novel generation adversarial network framework with characteristics aggregation and diffusion for brain disease classification and feature selection. *Briefings in Bioinformatics*, *23*(6), bbac454.

Bi, Xia-An, Wang, Yu, Luo, Sheng, Chen, Ke, Xing, Zhaoxu, & Xu, Luyun (2022). Hypergraph structural information aggregation generative adversarial networks for diagnosis and pathogenetic factors identification of Alzheimer's disease with imaging genetic data. *IEEE Transactions on Neural Networks and Learning Systems*.

Bi, Xia-An, Yang, Zicheng, Huang, Yangjun, Chen, Ke, Xing, Zhaoxu, Xu, Luyun, et al. (2024). CE-GAN: Community evolutionary generative adversarial network for Alzheimer's disease risk prediction. *IEEE Transactions on Medical Imaging*.

Bi, Xia-an, Zhou, Wenyan, Luo, Sheng, Mao, Yuhua, Hu, Xi, Zeng, Bin, et al. (2022). Feature aggregation graph convolutional network based on imaging genetic data for diagnosis and pathogeny identification of Alzheimer's disease. *Briefings in Bioinformatics*, *23*(3), bbac137.

Biffi, Alessandro, Anderson, Christopher D, Desikan, Rahul S, Sabuncu, Mert, Cortellini, Lynelle, Schmansky, Nick, et al. (2010). Genetic variation and neuroimaging measures in Alzheimer disease. *Archives of Neurology*, *67*(6), 677–685.

Bohbot, Véronique D, Lerch, Jason, Thorndycraft, Brook, Iaria, Giuseppe, & Zijdenbos, Alex P (2007). Gray matter differences correlate with spontaneous strategies in a human virtual navigation task. *Journal of Neuroscience*, *27*(38), 10078–10083.

Cherninskyi, Andrii, Storozhuk, Maksim, Maximyuk, Oleksandr, Kulyk, Vyacheslav, & Krishtal, Oleg (2023). Triggering of major brain disorders by protons and ATP: The role of ASICs and P2X receptors. *Neuroscience Bulletin*, *39*(5), 845–862.

Consortium, International Human Genome Sequencing (2004). Finishing the euchromatic sequence of the human genome. *Nature*, *431*(7011), 931–945.

Cursano, Silvia, Battaglia, Chiara R, Urrutia-Ruiz, Carolina, Grabrucker, Stefanie, Schön, Michael, Bockmann, Jürgen, et al. (2021). A CRHR1 antagonist prevents synaptic loss and memory deficits in a trauma-induced delirium-like syndrome. *Molecular Psychiatry*, *26*(8), 3778–3794.

de Leeuw, Christiaan A, Mooij, Joris M, Heskes, Tom, & Posthuma, Danielle (2015). MAGMA: generalized gene-set analysis of GWAS data. *PLoS Computational Biology*, *11*(4), Article e1004219.

Dosovitskiy, Alexey, Beyer, Lucas, Kolesnikov, Alexander, Weissenborn, Dirk, Zhai, Xiaohua, Unterthiner, Thomas, et al. (2020). An image is worth 16x16 words: Transformers for image recognition at scale. arXiv preprint arXiv:2010.11929.

Du, Lei, Liu, Kefei, Yao, Xiaohui, Risacher, Shannon L, Han, Junwei, Saykin, Andrew J, et al. (2020). Detecting genetic associations with brain imaging phenotypes in Alzheimer's disease via a novel structured SCCA approach. *Medical Image Analysis*, *61*, Article 101656.

Ewers, Michael, Luan, Ying, Frontzkowski, Lukas, Neitzel, Julia, Rubinski, Anna, Dichgans, Martin, et al. (2021). Segregation of functional networks is associated with cognitive resilience in Alzheimer's disease. *Brain*, *144*(7), 2176–2185.

Fair, Damien A, Schlaggar, Bradley L, Cohen, Alexander L, Miezin, Francis M, Dosenbach, Nico UF, Wenger, Kristin K, et al. (2007). A method for using blocked and event-related fMRI data to study "resting state" functional connectivity. *NeuroImage*, *35*(1), 396–405.

Fransson, Peter (2005). Spontaneous low-frequency BOLD signal fluctuations: An fMRI investigation of the resting-state default mode of brain function hypothesis. *Human Brain Mapping*, *26*(1), 15–29.

Furuya, TK, Silva, PNO, Payão, SLM, Bertolucci, PHF, Rasmussen, LT, De Labio, RW, et al. (2012). Analysis of SNAP25 mRNA expression and promoter DNA methylation in brain areas of Alzheimer's disease patients. *Neuroscience*, *220*, 41–46.

Gan, Jiangzhang, Peng, Ziwen, Zhu, Xiaofeng, Hu, Rongyao, Ma, Junbo, & Wu, Guorong (2021). Brain functional connectivity analysis based on multi-graph fusion. *Medical Image Analysis*, *71*, Article 102057.

Gao, Xingyu, Shi, Feng, Shen, Dinggang, & Liu, Manhua (2021). Task-induced pyramid and attention GAN for multimodal brain image imputation and classification in Alzheimer's disease. *IEEE Journal of Biomedical and Health Informatics*, *26*(1), 36–43.

Golovanevsky, Michal, Eickhoff, Carsten, & Singh, Ritambhara (2022). Multimodal attention-based deep learning for Alzheimer's disease diagnosis. *Journal of the American Medical Informatics Association*, *29*(12), 2014–2022.

Gonzales, Eric B., & Sumien, Nathalie (2017). Acidity and acid-sensing ion channels in the normal and Alzheimer's disease brain. *Journal of Alzheimer's Disease*, *57*(4), 1137–1144.

Greber, Susi, Lubec, Gert, Cairns, Nigel, & Fountoulakis, Michael (1999). Decreased levels of synaptosomal associated protein 25 in the brain of patients with down syndrome and Alzheimer's disease. *ELECTROPHORESIS: An International Journal*, *20*(4–5), 928–934.

Greenlaw, Keelin, Szefer, Elena, Graham, Jinko, Lesperance, Mary, Nathoo, Farouk S, & Initiative, Alzheimer's Disease Neuroimaging (2017). A Bayesian group sparse multi-task regression model for imaging genetics. *Bioinformatics*, *33*(16), 2513–2522.

He, Kaiming, Chen, Xinlei, Xie, Saining, Li, Yanghao, Dollár, Piotr, & Girshick, Ross (2022). Masked autoencoders are scalable vision learners. In *Proceedings of the IEEE/CVF conference on computer vision and pattern recognition* (pp. 16000–16009).

Hindriks, Rikkert, Adhikari, Mohit H, Murayama, Yusuke, Ganzetti, Marco, Mantini, Dante, Logothetis, Nikos K, et al. (2016). Can sliding-window correlations reveal dynamic functional connectivity in resting-state fMRI? *NeuroImage*, *127*, 242–256.

Hinds, David A, Kloek, Andrew P, Jen, Michael, Chen, Xiyin, & Frazer, Kelly A (2006). Common deletions and SNPs are in linkage disequilibrium in the human genome. *Nature Genetics*, *38*(1), 82–85.

Hu, Zhentao, Wang, Zheng, Jin, Yong, & Hou, Wei (2023). VGG-tswinformer: Transformer-based deep learning model for early Alzheimer's disease prediction. *Computer Methods and Programs in Biomedicine*, *229*, Article 107291.

Jack, Jr., Clifford R, Bernstein, Matt A, Fox, Nick C, Thompson, Paul, Alexander, Gene, Harvey, Danielle, et al. (2008). The Alzheimer's disease neuroimaging initiative (ADNI): MRI methods. *Journal of Magnetic Resonance Imaging: An Official Journal of the International Society for Magnetic Resonance in Medicine*, *27*(4), 685–691.

Jin, Shuting, Zeng, Xiangxiang, Xia, Feng, Huang, Wei, & Liu, Xiangrong (2021). Application of deep learning methods in biological networks. *Briefings in Bioinformatics*, *22*(2), 1902–1917.

Kan, Xuan, Dai, Wei, Cui, Hejie, Zhang, Zilong, Guo, Ying, & Yang, Carl (2022). Brain network transformer. *Advances in Neural Information Processing Systems*, *35*, 25586–25599.

Kong, Youyong, Gao, Shuwen, Yue, Yingying, Hou, Zhenhua, Shu, Huazhong, Xie, Chunming, et al. (2021). Spatio-temporal graph convolutional network for diagnosis and treatment response prediction of major depressive disorder from functional connectivity. *Human Brain Mapping*, *42*(12), 3922–3933.

Li, Gang, Han, Depeng, Wang, Chao, Hu, Wenxing, Calhoun, Vince D, & Wang, Yu-Ping (2020). Application of deep canonically correlated sparse autoencoder for the classification of schizophrenia. *Computer Methods and Programs in Biomedicine*, *183*, Article 105073.

Li, Yiming, Zeng, Min, Zhang, Fuhao, Wu, Fang-Xiang, & Li, Min (2023). DeepCellEss: cell line-specific essential protein prediction with attention-based interpretable deep learning. *Bioinformatics*, *39*(1), btac779.

Liu, Ze, Lin, Yutong, Cao, Yue, Hu, Han, Wei, Yixuan, Zhang, Zheng, et al. (2021). Swin transformer: Hierarchical vision transformer using shifted windows. In *Proceedings of the IEEE/CVF international conference on computer vision* (pp. 10012–10022).

Liu, Linfeng, Liu, Siyu, Zhang, Lu, To, Xuan Vinh, Nasrallah, Fatima, & Chandra, Shekhar S (2023). Cascaded multi-modal mixing transformers for Alzheimer's disease classification with incomplete data. *NeuroImage*, *277*, Article 120267.

Lundberg, Scott M., & Lee, Su-In (2017). A unified approach to interpreting model predictions. In *Advances in neural information processing systems: vol. 30*.

Mahmud, Mufti, Kaiser, M Shamim, McGinnity, T Martin, & Hussain, Amir (2021). Deep learning in mining biological data. *Cognitive Computation*, *13*, 1–33.

Mango, Dalila, & Nisticò, Robert (2021). Neurodegenerative disease: what potential therapeutic role of acid-sensing ion channels? *Frontiers in Cellular Neuroscience*, *15*, Article 730641.

Marees, Andries T, de Kluiver, Hilde, Stringer, Sven, Vorspan, Florence, Curis, Emmanuel, Marie-Claire, Cynthia, et al. (2018). A tutorial on conducting genome-wide association studies: Quality control and statistical analysis. *International Journal of Methods in Psychiatric Research*, *27*(2), Article e1608.

Meng, Guofeng, Xu, Hong, Lu, Dong, Li, Shensuo, Zhao, Zhenzhen, Li, Haohao, et al. (2023). Three-dimensional chromatin architecture datasets for aging and Alzheimer's disease. *Scientific Data*, *10*(1), 51.

Micheloyannis, Sifis, Sakkalis, Vagelis, Vourkas, Michalis, Stam, Cornelis J, & Simos, Panagiotis G (2005). Neural networks involved in mathematical thinking: evidence from linear and non-linear analysis of electroencephalographic activity. *Neuroscience Letters*, *373*(3), 212–217.

Peng, Wei, Chen, Tielin, & Dai, Wei (2021). Predicting drug response based on multi-omics fusion and graph convolution. *IEEE Journal of Biomedical and Health Informatics*, *26*(3), 1384–1393.

Peng, Wei, Tang, Qi, Dai, Wei, & Chen, Tielin (2022). Improving cancer driver gene identification using multi-task learning on graph convolutional network. *Briefings in Bioinformatics*, *23*(1), bbab432.

Purcell, Shaun, Neale, Benjamin, Todd-Brown, Kathe, Thomas, Lori, Ferreira, Manuel AR, Bender, David, et al. (2007). PLINK: a tool set for whole-genome association and population-based linkage analyses. *The American Journal of Human Genetics*, *81*(3), 559–575.

Qin, Zhiwei, Liu, Zhao, Guo, Qihao, & Zhu, Ping (2022). 3D convolutional neural networks with hybrid attention mechanism for early diagnosis of Alzheimer's disease. *Biomedical Signal Processing and Control*, *77*, Article 103828.

Qiu, Shangran, Miller, Matthew I, Joshi, Prajakta S, Lee, Joyce C, Xue, Chonghua, Ni, Yunruo, et al. (2022). Multimodal deep learning for Alzheimer's disease dementia assessment. *Nature Communications*, *13*(1), 3404.

Rosenberg, Paul B., Nowrangi, Milap A., & Lyketsos, Constantine G. (2015). Neuropsychiatric symptoms in Alzheimer's disease: What might be associated brain circuits? *Molecular Aspects of Medicine*, *43*, 25–37.

Roshchupkin, Gennady V, Adams, Hieab H, van der Lee, Sven J, Vernooij, Meike W, van Duijn, Cornelia M, Uitterlinden, Andre G, et al. (2016). Fine-mapping the effects of Alzheimer's disease risk loci on brain morphology. *Neurobiology of Aging*, *48*, 204–211.

Ruan, Ludan, & Jin, Qin (2022). Survey: Transformer based video-language pre-training. *AI Open*, *3*, 1–13.

Scelsi, Marzia A, Khan, Raiyan R, Lorenzi, Marco, Christopher, Leigh, Greicius, Michael D, Schott, Jonathan M, et al. (2018). Genetic study of multimodal imaging Alzheimer's disease progression score implicates novel loci. *Brain*, *141*(7), 2167–2180.

Shang, Junliang, Zou, Qi, Ren, Qianqian, Guan, Boxin, Li, Feng, Liu, Jin-Xing, et al. (2023). GCCN: Graph capsule convolutional network for progressive mild cognitive impairment prediction and pathogenesis identification based on imaging genetic data. *IEEE Journal of Biomedical and Health Informatics*.

Sharma, Rahul, Goel, Tripti, Tanveer, M, Lin, CT, & Murugan, R (2023). Deep learning based diagnosis and prognosis of Alzheimer's disease: A comprehensive review. *IEEE Transactions on Cognitive and Developmental Systems*.

Smith, Stephen M, Douaud, Gwenaëlle, Chen, Winfield, Hanayik, Taylor, Alfaro-Almagro, Fidel, Sharp, Kevin, et al. (2021). An expanded set of genome-wide association studies of brain imaging phenotypes in UK biobank. *Nature Neuroscience*, *24*(5), 737–745.

Song, Xiaofan, Mao, Mingyi, & Qian, Xiaohua (2021). Auto-metric graph neural network based on a meta-learning strategy for the diagnosis of Alzheimer's disease. *IEEE Journal of Biomedical and Health Informatics*, *25*(8), 3141–3152.

Stam, Cornelis J, van Walsum, Anne-Marie van Cappellen, & Micheloyannis, Sifis (2002). Variability of EEG synchronization during a working memory task in healthy subjects. *International Journal of Psychophysiology*, *46*(1), 53–66.

Szklarczyk, Damian, Kirsch, Rebecca, Koutrouli, Mikaela, Nastou, Katerina, Mehryary, Farrokh, Hachilif, Radja, et al. (2023). The STRING database in 2023: protein–protein association networks and functional enrichment analyses for any sequenced genome of interest. *Nucleic Acids Research*, *51*(D1), D638–D646.

Tanveer, Muhammad, Richhariya, Bharat, Khan, Riyaj Uddin, Rashid, Ashraf Haroon, Khanna, Pritee, Prasad, Mukesh, et al. (2020). Machine learning techniques for the diagnosis of Alzheimer's disease: A review. *ACM Transactions on Multimedia Computing, Communications, and Applications (TOMM)*, *16*(1s), 1–35.

Teipel, Stefan J, Fritz, H-Christian, Grothe, Michel J, & Initiative, Alzheimer's Disease Neuroimaging (2020). Neuropathologic features associated with basal forebrain atrophy in Alzheimer disease. *Neurology*, *95*(10), e1301–e1311.

Tian, Xu, Liu, Yan, Wang, Ling, Zeng, Xiangzhu, Huang, Yulang, & Wang, Zeng (2023). An extensible hierarchical graph convolutional network for early Alzheimer's disease identification. *Computer Methods and Programs in Biomedicine*, *238*, Article 107597.

Tzourio-Mazoyer, Nathalie, Landeau, Brigitte, Papathanassiou, Dimitri, Crivello, Fabrice, Etard, Octave, Delcroix, Nicolas, et al. (2002). Automated anatomical labeling of activations in SPM using a macroscopic anatomical parcellation of the MNI MRI single-subject brain. *NeuroImage*, *15*(1), 273–289.

Vaswani, Ashish, Shazeer, Noam, Parmar, Niki, Uszkoreit, Jakob, Jones, Llion, Gomez, Aidan N, et al. (2017). Attention is all you need. In *Advances in neural information processing systems*: *vol. 30*.

Wang, Wei, Han, Ruijiang, Zhang, Menghan, Wang, Yuxian, Wang, Tao, Wang, Yongtian, et al. (2022). A network-based method for brain disease gene prediction by integrating brain connectome and molecular network. *Briefings in Bioinformatics*, *23*(1), bbab459.

Wang, Jade Xiaoqing, Li, Yimei, Li, Xintong, & Lu, Zhao-Hua (2022). Alzheimer's disease classification through imaging genetic data with ignet. *Frontiers in Neuroscience*, *16*, Article 846638.

Wang, Hua, Nie, Feiping, Huang, Heng, Kim, Sungeun, Nho, Kwangsik, Risacher, Shannon L, et al. (2012). Identifying quantitative trait loci via group-sparse multitask regression and feature selection: an imaging genetics study of the adni cohort. *Bioinformatics*, *28*(2), 229–237.

Wang, Meiling, Shao, Wei, Hao, Xiaoke, Huang, Shuo, & Zhang, Daoqiang (2022). Identify connectome between genotypes and brain network phenotypes via deep self-reconstruction sparse canonical correlation analysis. *Bioinformatics*, *38*(8), 2323–2332.

Wei, Kai, Kong, Wei, & Wang, Shuaiqun (2022). Associating brain imaging phenotypes and genetic in Alzheimer's disease via JSCCA approach with autocorrelation constraints. *Medical & Biological Engineering & Computing*, *60*, 95–108.

West, Mark J, Coleman, Paul D, Flood, Dorothy G, & Troncoso, Juan C (1994). Differences in the pattern of hippocampal neuronal loss in normal ageing and Alzheimer's disease. *The Lancet*, *344*(8925), 769–772.

Xing, Xin, Liang, Gongbo, Blanton, Hunter, Rafique, Muhammad Usman, Wang, Chris, Lin, Ai-Ling, et al. (2020). Dynamic image for 3d mri image Alzheimer's disease classification. In *European conference on computer vision* (pp. 355–364). Springer.

Yan, Chao-Gan, Wang, Xin-Di, Zuo, Xi-Nian, & Zang, Yu-Feng (2016). DPABI: data processing & analysis for (resting-state) brain imaging. *Neuroinformatics*, *14*, 339–351.

Yan, Chaogan, & Zang, Yufeng (2010). DPARSF: a MATLAB toolbox for" pipeline" data analysis of resting-state fMRI. *Frontiers in Systems Neuroscience*, *4*, 1377.

Yi, Pan, Jin, Liu, Xu, Tian, Wei, Lan, & Rui, Guo (2021). Hippocampal segmentation in brain mri images using machine learning methods: A survey. *Chinese Journal of Electronics*, *30*(5), 793–814.

Yu, Meichen, Sporns, Olaf, & Saykin, Andrew J. (2021). The human connectome in Alzheimer disease—relationship to biomarkers and genetics. *Nature Reviews Neurology*, *17*(9), 545–563.

Zhang, Xin, Han, Liangxiu, Zhu, Wenyong, Sun, Liang, & Zhang, Daoqiang (2021). An explainable 3D residual self-attention deep neural network for joint atrophy localization and Alzheimer's disease diagnosis using structural MRI. *IEEE Journal of Biomedical and Health Informatics*, *26*(11), 5289–5297.

Zhao, Xingzhong, Song, Liting, Yang, Anyi, Zhang, Zichao, Zhang, Jinglong, Yang, Yucheng T, et al. (2023). Prioritizing genes associated with brain disorders by leveraging enhancer-promoter interactions in diverse neural cells and tissues. *Genome Medicine*, *15*(1), 56.

Zhou, Tao, Thung, Kim-Han, Liu, Mingxia, Shi, Feng, Zhang, Changqing, & Shen, Dinggang (2020). Multi-modal latent space inducing ensemble SVM classifier for early dementia diagnosis with neuroimaging data. *Medical Image Analysis*, *60*, Article 101630.

Zhou, Yingyao, Zhou, Bin, Pache, Lars, Chang, Max, Khodabakhshi, Alireza Hadj, Tanaseichuk, Olga, et al. (2019). Metascape provides a biologist-oriented resource for the analysis of systems-level datasets. *Nature Communications*, *10*(1), 1523.